

Gravitational lensing for a boosted Kerr black hole in the presence of plasma

Carlos A. Benavides-Gallego¹, A. A. Abdujabbarov^{1,2}, and
Cosimo Bambi^{1,3,a}

¹Center for Field Theory and Particle Physics and Department of Physics, Fudan University, 200438 Shanghai, China

²Ulugh Beg Astronomical Institute, Astronomicheskaya 33, Tashkent 100052, Uzbekistan

³Theoretical Astrophysics, Eberhard-Karls Universität Tübingen, 72076 Tübingen, Germany

the date of receipt and acceptance should be inserted later

Abstract We obtain the deflection angle for a boosted Kerr black hole in the weak field approximation. We also study the behavior of light in the presence of plasma by considering different distributions: singular isothermal sphere, non-singular isothermal gas sphere, and plasma in a galaxy cluster. We find that the dragging of the inertial system along with the boosted parameter Λ affect the value of the deflection angle. As an application, we studied the magnification for both uniform and **SIS** distributions.

Keywords boosted Kerr metric, gravitational lensing, inhomogeneous plasma distributions

1 Introduction

The revolutionary detection of gravitational waves from the coalescence of two black holes showed the formation of rapidly rotating black hole boosted with linear velocity [1, 2, 3]. The possible observation of the electromagnetic counterpart from black hole merger could provide more information about angular and linear momentum of the black hole in such systems [4, 5]. This fact indicates the importance of the inclusion of the boost parameter to Kerr spacetimes in order to study the effects of the boost velocity to the geometry (gravitational field) around a black hole. The solution of Einstein's vacuum field equations describing a boosted Kerr black hole relative to an asymptotic Lorentz frame at future null infinity was obtained in [6]. The electromagnetic structure around a boosted black hole has been studied in [4]. The author of Ref. [5] has considered the solution of Maxwell equations in the background geometry of a boosted black hole. In the present paper, we study

weak gravitational lensing around a boosted black hole described by the solution in [6].

The gravitational lensing effect is a good tool to test Einstein's theory of general relativity. For a review on light propagation in the curved spacetime and geometrical optics in general relativity, see e.g. [7, 8, 9, 10]. The photon motion is also affected by the presence of a plasma and the effect of plasma around a compact objects on lensing effects has been studied in [11, 12, 13, 14, 15, 16, 17, 18, 19, 20, 21, 22, 23, 24, 25, 26, 27, 28, 29, 30, 31]. In the literature, we can find a lot of work devoted to another optical property of black holes, the so-called black hole shadow [32, 33, 34, 35, 36, 37, 36, 38, 39, 40, 41, 42, 43, 44, 45, 46, 47, 48, 49, 50, 51, 52, 53, 54, 55, 56, 57, 58, 59, 60, 61, 62, 63, 64].

Starting from [65, 66, 67, 68, 69], there is a rich literature on weak gravitational lensing. Strong gravitational lensing around spherically symmetric compact objects is described in [70, 71].

In the present paper, we study weak lensing around a boosted black hole in the presence of plasma. The paper is organized as follow. In Section 2, we briefly review the optics in curved spacetime and describe the procedure to obtain the deflection angle in the weak field approximation following [22, 25]. In Section 3, we present the boosted Kerr metric in both diagonal and non-diagonal cases (non-rotating and slowly rotating cases, respectively). In Subsections 4.1 and 4.2, we find the expression for the deflection angle. Then, in section 5, we study the deflection angle in the presence of plasma, both for uniform and non-uniform distributions. For the inhomogeneous case, we consider three distribution models: singular isothermal sphere (**SIS**), non-singular isothermal sphere (**NSIS**), and the case of a plasma in a galaxy cluster (**PGC**). Finally, as an application, we devote section 6 to study the magnifi-

^a e-mail: bambi@fudan.edu.cn

cation for the uniform and **SIS** plasma distributions.

Throughout the paper we use the convention in which Greek indices run from 0 to 3, while Latin indices run from 1 to 3. Moreover, with the exception of Section 2, we use geometrized units, where $c = G = 1$.

2 Optics in a curved space-time

In this section, we review the optics in a curved space-time developed by Synge in 1960 [7]. Let us consider a static spacetime metric describing a weak gravitational field in an asymptotically flat spacetime. The metric coefficients can be written as [22, 25, 72]

$$g_{\alpha\beta} = \eta_{\alpha\beta} + h_{\alpha\beta} , \quad (1)$$

$$g^{\alpha\beta} = \eta^{\alpha\beta} - h^{\alpha\beta} , \quad (2)$$

where $\eta_{\alpha\beta}$ is the metric of the Minkowski spacetime, $h_{\alpha\beta} \ll 1$, $h_{\alpha\beta} \rightarrow 0$ for $x^\alpha \rightarrow \infty$, and $h^{\alpha\beta} = h_{\alpha\beta}$.

Using this approach for the static case, the phase velocity¹ u and the 4-vector of the photon momentum p^α are related by the following equation [7]

$$\frac{c^2}{u^2} = n^2 = 1 + \frac{p_\alpha p^\alpha}{(p^0 \sqrt{-g_{00}})^2} . \quad (4)$$

In order to obtain the photon trajectories in the presence of a gravitational field, one can modify the Fermat's least action principle for the light propagation by considering a dispersive medium [7]. Then, using the Hamiltonian formalism, it is easy to show that the variational principle

$$\delta \left(\int p_\alpha dx^\alpha \right) = 0 , \quad (5)$$

with the condition

$$W(x^\alpha, p_\alpha) = \frac{1}{2} \left[g^{\alpha\beta} p_\alpha p_\beta - (n^2 - 1) \left(p_0 \sqrt{-g_{00}} \right)^2 \right] = 0 ,$$

leads to the following system of differential equations that describes the trajectories of photons

$$\begin{aligned} \frac{dx^\alpha}{d\lambda} &= \frac{\partial W}{\partial p_\alpha} , \\ \frac{dp_\alpha}{d\lambda} &= - \frac{\partial W}{\partial x^\alpha} , \end{aligned} \quad (6)$$

¹The phase velocity is defined as the minimum value of [7]

$$u'^2 = 1 + \frac{dx_\alpha dx^\alpha}{(V_\beta dx^\beta)^2} , \quad (3)$$

where u' is the velocity of a fictitious particle riding on the wave front relative to a time-like world-line C (intersecting the wave) of an observer with 4-velocity V^μ (see [7] for details).

with the affine parameter λ changing along the light trajectory. Note that the scalar function $W(x^\alpha, p_\alpha)$ has been defined by means of Eq. (4).

In the Refs. [22, 25], it has been considered a static inhomogeneous plasma with a refraction index n which depends on the space location x^i

$$n^2 = 1 - \frac{\omega_e^2}{[\omega(x^i)]^2} , \quad (7)$$

$$\omega_e^2 = \frac{4\pi e^2 N(x^i)}{m} = K_e N(x^i) , \quad (8)$$

where $\omega(x^i)$ is the frequency of the photon that, due to gravitational redshift, depends on the space coordinates x^1, x^2, x^3 , e is the electron charge, m is the electron mass, ω_e is the electron plasma frequency, and $N(x^i)$ is the electron concentration in an inhomogeneous plasma [22].

According to Synge [7], for the case of a static medium in a static gravitational field, one can express the photon energy as

$$p_0 \sqrt{-g^{00}} = -\frac{1}{c} \hbar \omega(x^i) . \quad (9)$$

Using Eq. (7) one can express the scalar function $W(x^\alpha, p_\alpha)$ in the following form

$$W(x^\alpha, p_\alpha) = \frac{1}{2} \left[g^{\alpha\beta} p_\alpha p_\beta + \frac{\omega_e^2 \hbar^2}{c^2} \right] , \quad (10)$$

where \hbar is the Planck's constant. The scalar function expressed in Eq. (10) has been used in Refs. [22, 25] to find the equations of light propagation for diagonal and non-diagonal spacetimes.

In contrast with the case of a flat spacetime in vacuum, where the solution for photon's trajectory is a straight line, the presence of an arbitrary medium in curved spacetimes makes photons move along bent trajectories. However, taking into account only small deviations, it is possible to use the components of the 4-momentum of the photon moving in a straight line along the z -axis as an approximation. This components are given by (see, e.g. [22, 25])

$$p^\alpha = \left(\frac{\hbar \omega}{c}, 0, 0, \frac{n \hbar \omega}{c} \right) , \quad (11)$$

$$p_\alpha = \left(-\frac{\hbar \omega}{c}, 0, 0, \frac{n \hbar \omega}{c} \right) . \quad (12)$$

Eqs. (11) and (12) are known as the null approximation. It is important to point out that both ω and n are evaluated at ∞ . In this sense, we have introduced the notation in which

$$\begin{aligned} \omega &= \omega(\infty) \\ n &= n(\infty) . \end{aligned} \quad (13)$$

This notation has been also used in [22, 25], and will be used along the manuscript.

2.1 Equations of light propagation in a diagonal spacetime

First, we consider the spacetime with a diagonal metric tensor. In this spacetime, the components of the metric tensor $g_{\alpha\beta}$ vanish for $\alpha \neq \beta$. Hence, after using Eq. (10), the system in (6) can be expressed as [22]

$$\begin{aligned} \frac{dx^i}{d\lambda} &= g^{ij} p_j, \\ \frac{dp_i}{d\lambda} &= -\frac{1}{2} g^{lm}{}_{,i} p_l p_m - \frac{1}{2} g^{00}{}_{,i} p_0^2 - \frac{1}{2} \frac{\hbar^2}{c^2} K_e N_{,i}. \end{aligned} \quad (14)$$

Then, with the aid of the null approximation, the first equation in (14) reduces to

$$\frac{dz}{d\lambda} = \frac{n\hbar\omega}{c}. \quad (15)$$

In the null approximation, the 3-vector in the direction of the photon momentum is written as $e^i = e_i = (0, 0, 1)$. Therefore p_i can be expressed as

$$p_i = \frac{n\hbar\omega}{c} (0, 0, 1) = \frac{n\hbar\omega}{c} e_i. \quad (16)$$

Hence, the second equation in (14) can be expressed by

$$\begin{aligned} \frac{d}{d\lambda} \left(\frac{n\hbar\omega}{c} e_i \right) &= -\frac{1}{2} g^{lm}{}_{,i} p_l p_m \\ &\quad - \frac{1}{2} g^{00}{}_{,i} p_0^2 - \frac{1}{2} \frac{\hbar^2}{c^2} K_e N_{,i}. \end{aligned} \quad (17)$$

Then, after using Eq. (15) and differentiating, the last expression takes the form

$$\begin{aligned} \frac{de_i}{dz} &= -\frac{1}{2} \frac{c^2}{n\hbar^2\omega^2} \left(g^{00}{}_{,i} (p_0)^2 + g^{lm}{}_{,i} p_l p_m + \frac{\hbar^2}{c^2} K_e N_{,i} \right) \\ &\quad - e_i \frac{dn}{dz}. \end{aligned} \quad (18)$$

In Ref. [22], only those components of the 3-vector that are perpendicular to the initial direction of propagation were taken into account. In this sense, the contribution to the deflection of photons is due only to the change in e_1 and e_2 . Hence, after using the null approximation $e_i = 0$ along with the assumption of weak gravitational field, Eq. (18) reduces to

$$\frac{de_i}{dz} = \frac{1}{2} \left(h_{33,i} + \frac{1}{n^2} h_{00,i} - \frac{1}{n^2\omega^2} K_e N_{,i} \right), \quad (19)$$

for $i = 1, 2$.

The deflection angle is determined by the change of the 3-vector e_i . This means that

$$\hat{\alpha} = \mathbf{e}(+\infty) - \mathbf{e}(-\infty). \quad (20)$$

Then, using Eq. (19), the deflection angle becomes

$$\hat{\alpha}_i = \frac{1}{2} \int_{-\infty}^{\infty} \left(h_{33,i} + \frac{\omega^2}{\omega^2 - \omega_e^2} h_{00,i} - \frac{K_e}{\omega^2 - \omega_e^2} N_{,i} \right) dz, \quad (21)$$

for $i = 1, 2$. In the last expression ω_e and n are evaluated at infinity, and $\omega(\infty) = \omega$ [22]. In terms of the impact parameter b , Eq. (21) takes the form [22]

$$\hat{\alpha}_b = \frac{1}{2} \int_{-\infty}^{\infty} \frac{b}{r} \left(\frac{dh_{33}}{dr} + \frac{1}{1 - \omega_e^2/\omega^2} \frac{dh_{00}}{dr} - \frac{K_e}{\omega^2 - \omega_e^2} \frac{dN}{dr} \right), \quad (22)$$

where $r = \sqrt{b^2 + z^2}$.

2.2 Equations of light propagation in a non-diagonal spacetime

Now we consider a spacetime with a non-diagonal metric tensor; that is, the components of metric tensor $g_{\alpha\beta}$ do not vanish for $\alpha \neq \beta$. Therefore, the scalar function $W(x^\alpha, p_\alpha)$ in Eq. (10) can be expressed as [25]

$$W(x^\alpha, p_\alpha) = \frac{1}{2} \left[g^{00} p_0^2 + 2g^{0l} p_0 p_l + g^{lm} p_l p_m + \frac{\omega_e^2 \hbar^2}{c^2} \right]. \quad (23)$$

Hence, the system of differential equations in (6) takes the form

$$\frac{dx^i}{d\lambda} = g^{ij} p_j \quad (24)$$

$$\begin{aligned} \frac{dp_i}{d\lambda} &= -\frac{1}{2} g^{lm}{}_{,i} p_l p_m - \frac{1}{2} g^{00}{}_{,i} p_0^2 - g^{0l}{}_{,i} p_0 p_l \\ &\quad - \frac{1}{2} \frac{\hbar^2}{c^2} K_e N_{,i}. \end{aligned} \quad (25)$$

Then, using Eq. (15) and assuming that the gravitational field is weak, we obtain

$$\begin{aligned} \frac{dp_i}{dz} &= \frac{1}{2} \frac{n\hbar\omega}{c} \\ &\quad \times \left(h_{33,i} + \frac{1}{n^2} h_{00,i} + \frac{1}{n} h_{03,i} - \frac{K_e N_{,i}}{n^2\omega^2} \right). \end{aligned} \quad (26)$$

Therefore, following the procedure in Subsection 2.1, the deflection angle for a non-diagonal spacetime in the weak limit has the form

$$\begin{aligned} \hat{\alpha}_i &= \frac{1}{2} \int_{-\infty}^{\infty} \left(h_{33,i} + \frac{\omega^2}{\omega^2 - \omega_e^2} h_{00,i} + \frac{1}{n} h_{03,i} \right. \\ &\quad \left. - \frac{K_e N_{,i}}{\omega^2 - \omega_e^2} \right) dz. \end{aligned} \quad (27)$$

3 Boosted Kerr metric

The boosted Kerr metric, which describes a boosted black hole relative to an asymptotic Lorentz frame, is a solution of Einstein's vacuum field equations obtained in [6]. This solution has three parameters: mass, rotation and boost. In Kerr-Schild coordinates, the line element reads

$$ds^2 = - \left(1 - \frac{2Mr}{\Sigma}\right) dt'^2 + \left(1 + \frac{2Mr}{\Sigma}\right) dr^2 + \frac{\Sigma}{\Lambda} d\theta^2 + \frac{A \sin^2(\theta)}{\Lambda^2 \Sigma} d\phi^2 - \frac{4Mra \sin^2 \theta}{\Lambda \Sigma} dt' d\phi - \frac{4Mr}{\Sigma} dt' dr - \frac{2a \sin^2 \theta}{\Lambda} \left(1 - \frac{2Mr}{\Sigma}\right) dr d\phi, \quad (28)$$

with

$$\Sigma = r^2 + a^2 \left(\frac{\beta + \alpha \cos \theta}{\alpha + \beta \cos \theta} \right)^2, \quad (29)$$

$$\Lambda = (\alpha + \beta \cos \theta)^2, \quad (30)$$

$$A = \Sigma^2 + a^2 (\Sigma + 2Mr) \sin^2 \theta, \quad (31)$$

where $a = J/M$ is the specific angular momentum of the compact object with total mass M , $\alpha = \cosh \gamma$, $\beta = \sinh \gamma$, and γ is the usual Lorentz factor which defines the boost velocity v by the formula $v = \tanh \gamma = \beta/\alpha$. Note that the metric in (28) exactly reduces to the Kerr one when $\Lambda = 1$ ($v = 0$). It is also important to point out that the direction of the boost for the Kerr black hole is along the axis of rotation while for Schwarzschild is along the z -axis.

To study the deflection angle for the boosted Kerr metric in the presence of a medium, we consider both the non-rotating and the slowly rotating cases. In this sense, following the ideas in [22] and [25], we devote this section to find the form of the line element (28) in each case.

3.1 Boosted Kerr metric: non-rotating case

The non-rotating case is obtained by setting $a = 0$. Hence, the metric (28) reduces to

$$ds^2 = - \left(1 - \frac{2M}{r}\right) dt'^2 + \left(1 + \frac{2M}{r}\right) dr^2 + \frac{r^2}{\Lambda} d\theta^2 + \frac{\sin^2 \theta}{\Lambda^2} r^2 d\phi^2 - \frac{4M}{r} dt' dr. \quad (32)$$

In Ref. [22], Cartesian coordinates have been used to find the terms h_{ik} . Nevertheless, before changing the coordinates, we want to write the form of the metric in Eq. (32) for small values of the velocity ($v \ll 1$). In order to do so, we express $1/\Lambda$ and $1/\Lambda^2$ in terms

of v and consider a Taylor expansion up to first order. Therefore, the metric (32) takes the form

$$ds^2 = - \left(1 - \frac{2M}{r}\right) dt'^2 + \left(1 + \frac{2M}{r}\right) dr^2 + r^2(1 - 2v \cos \theta) d\theta^2 + r^2 \sin^2 \theta d\phi^2 - 4vr^2 \sin^2 \theta \cos \theta d\phi^2 - \frac{4M}{r} dt' dr. \quad (33)$$

Now, to transform the line element (33) into Boyer-Lindquist coordinates, we use the relation (see [73], page 15)

$$t' = t - 2M \ln \left(\frac{r}{2M} - 1 \right); \quad (34)$$

from which one can easily obtain

$$ds^2 = - \left(1 - \frac{2M}{r}\right) dt^2 + \left(1 - \frac{2M}{r}\right)^{-1} dr^2 + r^2 [(1 - 2v \cos \theta) d\theta^2 + (1 - 4v \cos \theta) \sin^2 \theta d\phi^2]. \quad (35)$$

In the weak field limit, the approximation is done by considering $2M/r \ll 1$. In this sense, according to [22], the main idea is to express the line element in Eq. (35) as

$$ds^2 = ds_0^2 + ds'^2 \quad (36)$$

where

$$ds_0^2 = -dt^2 + dr^2 + r^2(d\theta^2 + \sin^2 \theta d\phi^2), \quad (37)$$

is the flat space-time, and ds'^2 is the part of the metric containing the perturbation terms h_{ik} . Therefore, after considering the weak approximation, the line element (35) has the form

$$ds^2 = ds_0^2 + \frac{2M}{r} dt^2 + \frac{2M}{r} dr^2 - 2vr^2 \cos \theta d\theta^2 - 4vr^2 \cos \theta \sin^2 \theta d\phi^2. \quad (38)$$

Eq. (35) is the non-rotating boosted Kerr metric in the weak field approximation expressed in Boyer-Lindquist coordinates. In order to identify the components h_{ik} , we need to express the line element in Eq. (38) in Cartesian coordinates. After following the procedure described in Appendix I, we found that h_{00} and h_{33} are

$$h_{00} = \frac{2M}{r} \quad (39)$$

$$h_{33} = \frac{2M}{r} \cos^2 \theta - 2v \cos \theta \sin^2 \theta, \quad (40)$$

3.2 Boosted Kerr metric: rotating case

The spacetime describing a slowly rotating massive object was obtained in [74]. However, in this work, we use the form of the metric reported in [25]. Using geometrized units, this metric takes the form

$$ds^2 = -\left(1 - \frac{2M}{r}\right) dt^2 + \left(1 - \frac{2M}{r}\right)^{-1} dr^2 + r^2(d\theta^2 + \sin^2\theta d\phi^2) - 2\omega_{LT}r^2 \sin^2\theta dt d\phi, \quad (41)$$

where $\omega_{LT} = 2Ma/r^3 = 2J/r^3$ is the Lense-Thirring angular velocity of the dragging of inertial frames.

For the case of the boosted Kerr metric, the line element has the same form. Introducing the notation $\bar{\omega}_{LT} = 2\bar{J}/r^3$, where $\bar{J} = J/\Lambda$, one may obtain the “modified” metric of slowly rotating boosted velocity. Finally, the spacetime around boosted slowly rotating objects can be expressed by the following metric

$$ds^2 = -\left(1 - \frac{2M}{r}\right) dt^2 + \left(1 - \frac{2M}{r}\right)^{-1} dr^2 + r^2(d\theta^2 + \sin^2\theta d\phi^2) - 2\bar{\omega}_{LT}r^2 \sin^2\theta dt d\phi. \quad (42)$$

When $v = 0$, the expression in (42) reduces to that in [25].

4 Deflection angle in uniform plasma

4.1 Deflection of light for the non-rotating case

In Subsection 2.1, we discussed the procedure in [22] to obtain Eq. (22). Now, we apply this result to find the deflection angle for the boosted Kerr metric in the presence of a uniform plasma. We first consider the non-rotating case. From Eqs. (39) and (40) we have that

$$\frac{b}{r} \frac{dh_{00}}{dr} = -\frac{2Mb}{r^3} = -\frac{2Mb}{\sqrt{b^2 + z^2}^{\frac{3}{2}}}, \quad (43)$$

$$\begin{aligned} \frac{b}{r} \frac{dh_{33}}{dr} &= -\frac{6Mb}{r^5} z^2 + \frac{2bv}{r^3} z - \frac{6vb}{r^5} z^3 \\ &= -\frac{6Mb}{(b^2 + z^2)^{\frac{5}{2}}} z^2 + \frac{2bv}{(b^2 + z^2)^{\frac{3}{2}}} z \\ &\quad - \frac{6vb}{(b^2 + z^2)^{\frac{5}{2}}} z^3. \end{aligned} \quad (44)$$

Then, recalling that $\cos\theta = z/r$, $r = \sqrt{b^2 + z^2}$, and using Eq. (22), the deflection angle is

$$\begin{aligned} \hat{\alpha}_b &= -3Mb \int_{-\infty}^{\infty} \frac{z^2}{(b^2 + z^2)^{\frac{5}{2}}} dz \\ &\quad + bv \int_{-\infty}^{\infty} \frac{z}{(b^2 + z^2)^{\frac{3}{2}}} dz \\ &\quad - 3bv \int_{-\infty}^{\infty} \frac{z^3}{(b^2 + z^2)^{\frac{5}{2}}} dz \\ &\quad - Mb \int_{-\infty}^{\infty} \frac{\omega^2}{(\omega^2 - \omega_e^2)(b^2 + z^2)^{\frac{3}{2}}} dz \\ &\quad - \frac{bK_e}{2} \int_{-\infty}^{\infty} \frac{1}{\omega^2 - \omega_e^2} \frac{1}{r} \frac{dN}{dr} dz. \end{aligned} \quad (45)$$

Thus, after integration, we obtain

$$\begin{aligned} \hat{\alpha}_b &= \frac{2M}{b} + \frac{2Mb}{1 - \frac{\omega_e^2}{\omega^2}} \int_0^{\infty} \frac{dz}{(b^2 + z^2)^{\frac{3}{2}}} \\ &\quad + \frac{bK_e}{2} \int_{-\infty}^{\infty} \frac{1}{\omega^2 - \omega_e^2} \frac{1}{r} \frac{dN}{dr} dz. \end{aligned} \quad (46)$$

In the last expression, we took into account the symmetry of the limits (see appendix II for details). We also considered the fact that the deflection angle is defined as the difference between the initial and the final ray directions; that is, $\hat{\alpha} = \mathbf{e}_{in} - \mathbf{e}_{out}$. Therefore, it has the opposite sign (see [8]).

From Eq. (46) we note that, at first order, $\hat{\alpha}_b$ does not depend on the velocity. This is due to the fact that the second and third integrals in Eq. (45), which contain the dependence on v , vanish. If we consider a uniform plasma (ω_e constant), and the approximation $1 - n \ll \frac{\omega_e}{\omega}$, Eq. (46) reduces to [22]

$$\hat{\alpha}_b = \frac{2M}{b} \left(1 + \frac{1}{1 - \frac{\omega_e^2}{\omega^2}}\right). \quad (47)$$

In Fig. 1 left we plotted $\hat{\alpha}_b$ as a function of ω_e^2/ω^2 for different values of $b/2M$. The plot shows that $\hat{\alpha}_b$ increases as the ratio ω_e^2/ω^2 increases. On the other hand, for small values of $b/2M$ the values of the deflection angle are greater. For example, for $b/2M = 100$ the figure shows that $\hat{\alpha}_b$ is greater than 0.2; however, for $b/2M = 50, 100$ the deflection angle is less than 0.1. It is also possible to see from the figure that $\hat{\alpha}_b$ has the value $4M/b$ when there is not plasma ($\omega_e = 0$).

4.2 Deflection angle for the slowly rotating case

Due to the presence of non-diagonal terms in the line element (42), we use the form of the deflection angle

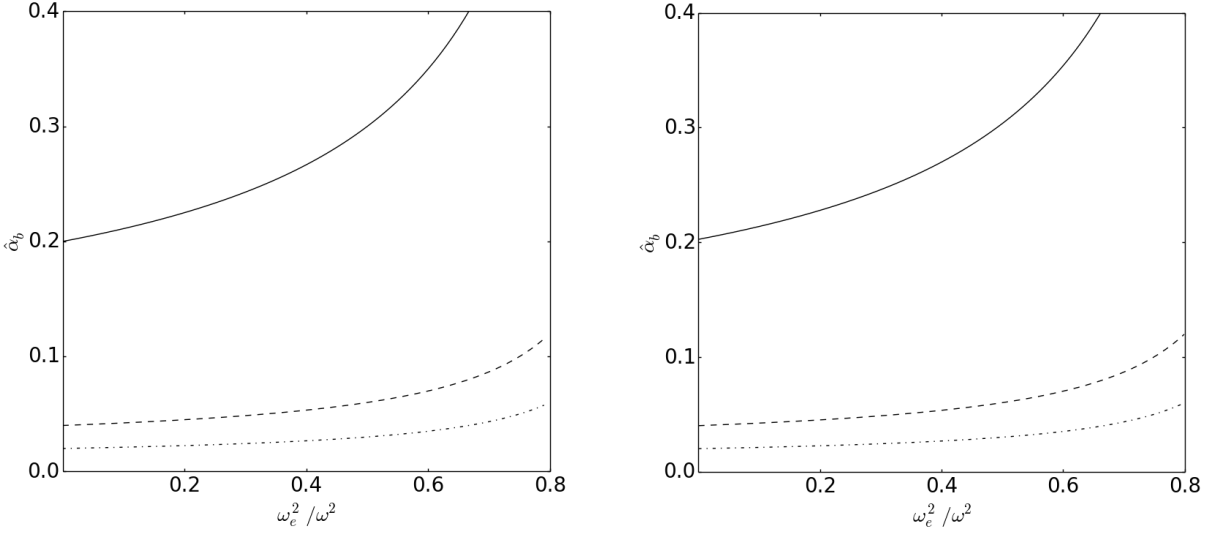


Fig. 1: **left:** Plot of $\hat{\alpha}_b$ vs. ω_e^2/ω^2 for $b/2M = 10$ (continuous line), $b/2M = 50$ (dashed line), and $b/2M = 100$ (dot-dashed line) for uniform plasma. **right:** Plot of $\hat{\alpha}_b$ vs. ω_e^2/ω^2 for the rotating case. We used different values of the impact parameter: $b/2M = 10$ (continuous line), $b/2M = 50$ (dashed line), and $b/2M = 100$ (dot-dashed line). We assumed $\Lambda = 0.5$, $J_r/M^2 = 0.25$, $\sin \chi = 1$, and $\omega_e^2/\omega^2 = 0.5$. Note that there is a small increment for $b/2M = 10$ when we compare with Schwarzschild (left panel).

in Eq. (27). According to [25], the effect of dragging of the inertial frame contributes to $\hat{\alpha}$ only by means of the projection \bar{J}_r of the angular momentum. Hence, after the introduction of polar coordinates (b, χ) on the intersection point between the light ray and the xy -plane, where χ is the angle between \mathbf{J}_r and \mathbf{b} , we find that [25] (see Fig. 2)

$$h_{03} = -2 \frac{\bar{J}_r b \sin \chi}{(b^2 + z^2)^{3/2}}. \quad (48)$$

Since Eq. (48) depends on χ and b , the deflection angle contains two contributions: the partial derivatives

$$\frac{\partial h_{03}}{\partial b} = -2 \bar{J}_r \sin \chi \left(\frac{1}{(b^2 + z^2)^{3/2}} - \frac{3b^2}{(b^2 + z^2)^{5/2}} \right), \quad (49)$$

$$\frac{\partial h_{03}}{\partial \chi} = -2 \frac{\bar{J}_r b \cos \chi}{(b^2 + z^2)^{3/2}}. \quad (50)$$

Thus, Eq. (27), for both contributions, takes the form

$$\hat{\alpha}_b = \hat{\alpha}_{bS} - 2 \bar{J}_r \sin \chi \times \int_0^\infty \left(\frac{1}{n(b^2 + z^2)^{3/2}} - \frac{3b^2}{n(b^2 + z^2)^{5/2}} \right) dz \quad (51)$$

$$\hat{\alpha}_\chi = -2 \bar{J}_r \cos \chi \int_0^\infty \frac{1}{n(b^2 + z^2)^{3/2}} dz, \quad (52)$$

where $\hat{\alpha}_{bS}$ is the deflection angle for Schwarzschild (see Eq. (46)). Therefore, considering an homogeneous plasma

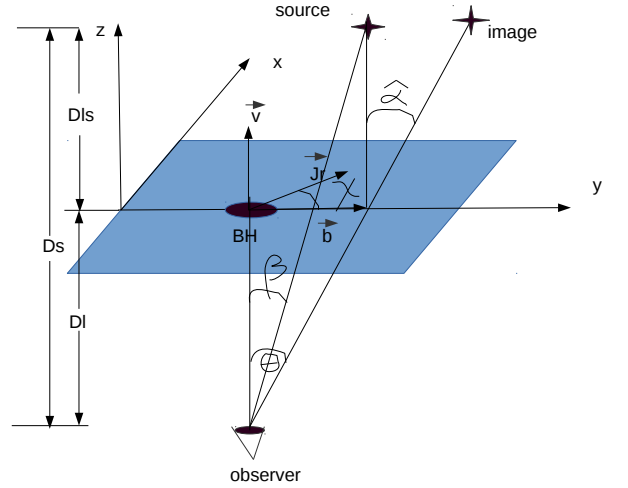


Fig. 2: Schematic representation of the gravitational lensing system. Here, χ represents the inclination angle between the vectors \mathbf{J}_r and \mathbf{b} . In the figure D_s , D_l , and D_{ls} are the distances from the source to the observer, from the lens to the observer, and from the source to the lens, respectively.

(constant value of ω_e), these contributions reduce to

$$\hat{\alpha}_b = \underbrace{\frac{2M}{b} \left(1 + \frac{1}{1 - \frac{\omega_e^2}{\omega^2}} \right)}_{\hat{\alpha}_{bS}} + \underbrace{\frac{1}{\sqrt{1 - \frac{\omega_e^2}{\omega^2}}} \frac{2J_r \sin \chi}{b^2 \Lambda}}_{\hat{\alpha}_{bD}} \quad (53)$$

$$\hat{\alpha}_\chi = -\frac{2J_r \cos \chi}{b^2 \Lambda \sqrt{1 - \frac{\omega_e^2}{\omega^2}}}; \quad (54)$$

where n was replaced by $\sqrt{1 - \frac{\omega_e^2}{\omega^2}}$. It is important to point out that Eq. (53) is only valid for $\omega > \omega_e$, because waves with $\omega < \omega_e$ do not propagate in the plasma [22, 75].

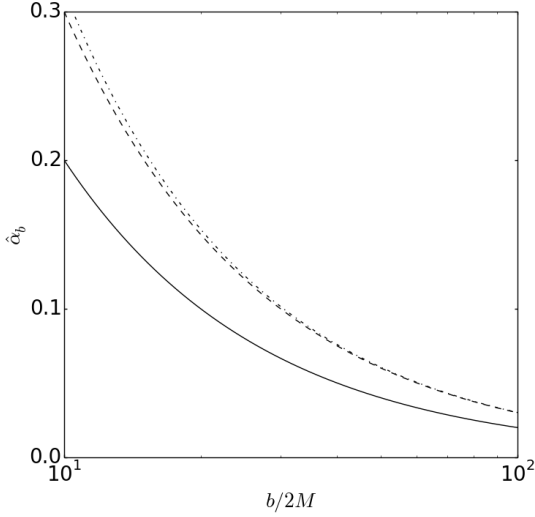


Fig. 3: Plot of $\hat{\alpha}_b$ vs. $b/2M$ in the presence of uniform plasma for the slowly rotating (dot-dashed line) and $\hat{\alpha}_{bS}$ (dashed line). In the figure it is also plotted the Schwarzschild case in vacuum (continuous line). We used $\Lambda = 0.5$, $J_r/M^2 = 0.25$, $\sin \chi = 1$, and $\omega_e^2/\omega^2 = 0.5$.

In Fig. 3, we plot $\hat{\alpha}_{bS}$ and $\hat{\alpha}_b$ for the slowly rotating case as a function of the impact parameter $b/2M$. From this figure, we can see that there is a difference between both angles. This means that $\hat{\alpha}_b$ for a boosted Kerr black hole is greater than $\hat{\alpha}_{bS}$. This is due to the rotation and boost velocity v , which is larger for small values of $b/2M$. On the other hand, for larger values of the impact parameter $b/2M$, this difference becomes very small, and both angles behave in the same way since $2J_r \sin \chi / (nb^2 \Lambda) \rightarrow 0$ when $b/2M \rightarrow \infty$.

Fig. 1 right shows $\hat{\alpha}_b$ as a function of ω_e^2/ω^2 . The behavior is very similar to that of Schwarzschild (Fig. 1

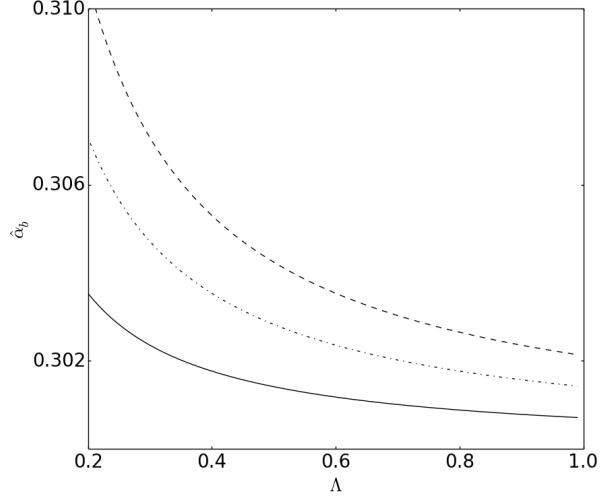


Fig. 4: Plot of $\hat{\alpha}_b$ vs. Λ for $J_r/M^2 = 0.1$ (continuous line), $J_r/M^2 = 0.2$ (dot-dashed line), and $J_r/M^2 = 0.3$ (dashed line). We assumed $b/2M = 10$, $\sin \chi = 1$, and $\omega_e^2/\omega^2 = 0.5$.

left). However, note that there is a small increment for $b/2M = 10$. On the other hand, we see that the deflection angle tends to $2M/b + 2J_r \sin \chi / (b^2 \Lambda)$ when there is not plasma ($\omega_e^2 = 0$).

In Fig. 4 we plotted Eq. (53) as a function of Λ for different values of J_r . We took into account the condition in which $0 < \Lambda \leq 1$ in order to give the values. In this figure, for different values of Λ , we see that $\hat{\alpha}_b$ is bigger when $\Lambda \rightarrow 0$. Moreover, for $\Lambda = 1$, the deflection angle reduces to the value $\hat{\alpha}_{bS} + 2J_r \sin \chi / nb^2$.

5 Models for the boosted Kerr metric with non-uniform plasma distribution

The deflection angle for a boosted Kerr metric in a non-uniform plasma was calculated in Subsection 4.2.

Hence, for $\omega_e^2/\omega^2 \ll 1$, Eq. (51) reduces to

$$\begin{aligned} \hat{\alpha}_b = & \underbrace{\frac{4M}{b}}_{\hat{\alpha}_{S1}} + \underbrace{\frac{2Mb}{\omega^2} \int_0^\infty \frac{\omega_e^2}{r^3} dz}_{\hat{\alpha}_{S2}} \\ & + \underbrace{\frac{bK_e}{\omega^2} \int_0^\infty \frac{1}{r} \frac{dN}{dr} dz}_{\hat{\alpha}_{S3}} + \underbrace{\frac{bK_e}{\omega^4} \int_0^\infty \frac{\omega_e^2}{r} \frac{dN}{dr} dz}_{\hat{\alpha}_{S4}} \\ & + \underbrace{\frac{2J_r}{\Lambda b^2} \sin \chi}_{\hat{\alpha}_{B1}} - \underbrace{\frac{J_r}{\Lambda \omega^2} \sin \chi \int_0^\infty \frac{\omega_e^2}{r^3} dz}_{\hat{\alpha}_{B2}} \\ & + \underbrace{\frac{3b^2 J_r}{\Lambda \omega^2} \sin \chi \int_0^\infty \frac{\omega_e^2}{r^5} dz}_{\hat{\alpha}_{B3}}, \end{aligned} \quad (55)$$

where $r = \sqrt{b^2 + z^2}$, and S and B stand for Schwarzschild and Boosted, respectively. Using Eq. (55), we calculate the deflection angle by considering different plasma distributions: singular isothermal sphere (**SIS**), non-singular isothermal gas sphere (**NSIS**), and a plasma in a galaxy cluster (**PGC**).

Eq. (55) is quite similar to that obtained in [22]. In this equation, we also find the vacuum gravitational deflection $\hat{\alpha}_{S1}$, the correction to the gravitational deflection due to the presence of the plasma $\hat{\alpha}_{S2}$, the refraction deflection due to the inhomogeneity of the plasma $\hat{\alpha}_{S3}$, and its small correction $\hat{\alpha}_{S4}$. Nevertheless, when the boosted Kerr metric is considered, three more terms appear: $\hat{\alpha}_{B1}$, $\hat{\alpha}_{B2}$, and $\hat{\alpha}_{B3}$. These are contributions due to the dragging of the inertial frame. The former is a constant that appears in all models considered, while the others two depend on the plasma distribution.

From now on, let us suppose that the vectors \mathbf{J}_r and \mathbf{b} are perpendicular to each other ($\cos \chi = 0$). Therefore, the contribution $\hat{\alpha}_\chi$ vanishes (see Eq. (54)) and $\sin \chi = 1$. Furthermore, since $\hat{\alpha}_{S4}$ is small, we neglect its contribution (see [22]).

5.1 Singular isothermal sphere

In this subsection, we consider the model for a singular isothermal sphere proposed in [76, 77]. In this model, often used in lens modelling of galaxies and clusters, the density distribution has the form

$$\rho(r) = \frac{\sigma_v^2}{2\pi r^2}, \quad (56)$$

where σ_v^2 is a one-dimensional velocity dispersion. The concentration of the plasma has the form

$$N(r) = \frac{\rho(r)}{\kappa m_p}, \quad (57)$$

where m_p is the proton mass and κ is a non-dimensional coefficient which is related to the dark matter contribution [22]. Using Eqs. (7) and (56) the plasma frequency is

$$\omega_e^2 = K_e N(r) = \frac{K_e \sigma_v^2}{2\pi \kappa m_p r^2}. \quad (58)$$

Then, from Eqs. (55) and (58), and the well known property of the Γ -function [78] (see Appendix II), the contributions to the deflection angle can be found in the form

$$\begin{aligned} \hat{\alpha}_{S2} &= \frac{1}{12\pi} \frac{\omega_c^2}{\omega^2 \bar{b}^3}, \quad \hat{\alpha}_{S3} = -\frac{1}{16} \frac{\omega_c^2}{\omega^2 \bar{b}^2} \\ \hat{\alpha}_{B2} &= -\frac{1}{48\pi} \frac{\tilde{J}_r \omega_c^2}{\Lambda \omega^2 \bar{b}^4}, \quad \hat{\alpha}_{B3} = \frac{1}{20\pi} \frac{\tilde{J}_r \omega_c^2}{\Lambda \omega^2 \bar{b}^4}. \end{aligned} \quad (59)$$

Where $\omega_c^2 = \frac{K_e \sigma_v^2}{M^2 \kappa m_p}$, $\tilde{J}_r = J_r/M^2$, and $\bar{b} = b/2M$. Hence deflection angle takes the form

$$\begin{aligned} \hat{\alpha}_{SIS} = & \frac{2}{\bar{b}} + \frac{1}{12\pi} \frac{\omega_c^2}{\omega^2 \bar{b}^3} - \frac{1}{16} \frac{\omega_c^2}{\omega^2 \bar{b}^2} + \frac{1}{2} \frac{\tilde{J}_r}{\Lambda \bar{b}^2} \\ & - \frac{1}{48\pi} \frac{\tilde{J}_r \omega_c^2}{\Lambda \omega^2 \bar{b}^4} + \frac{1}{20\pi} \frac{\tilde{J}_r \omega_c^2}{\Lambda \omega^2 \bar{b}^4} \end{aligned} \quad (60)$$

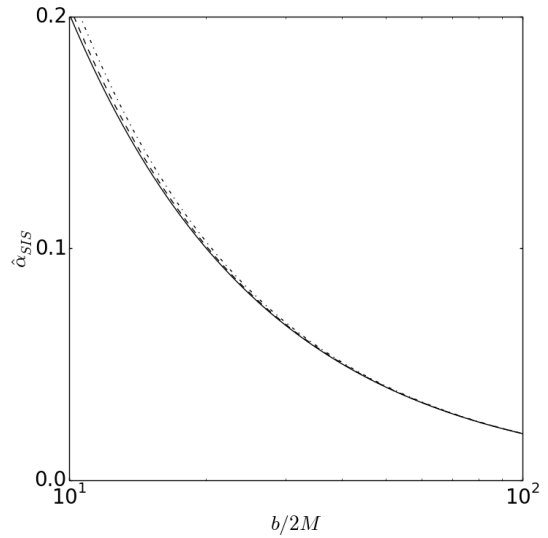


Fig. 5: Plot of $\hat{\alpha}_{SIS}$ vs. $b/2M$ for $\Lambda = 1$ (continuous line), $\Lambda = 0.2$ (dashed line), and $\Lambda = 0.1$ (dot-dashed line). We used $J_r/M^2 = 0.25$, $\sin \chi = 1$, and $\omega_e^2/\omega^2 = 0.5$.

In Fig. 5, we plot $\hat{\alpha}_{SIS}$ as a function of \bar{b} for different values of Λ . The figure does not show any difference for values of $b/2M$ greater than 10. However, for values of $b/2M$ near to 10, we see a small difference. This

means that $\hat{\alpha}_{SIS}$ is greater when Λ is small. For $\Lambda = 1$ ($v = 0$), we have the case of a slowly rotating massive object. Therefore, the parameter Λ has a small effect on the deflection angle. This tendency can be seen clearly in Fig. 6, where we plotted the behavior of the deflection angle as a function of Λ for different values of \tilde{J}_r . Note that the boosted parameter is constrained to be in the interval $0 < \Lambda \leq 1$.

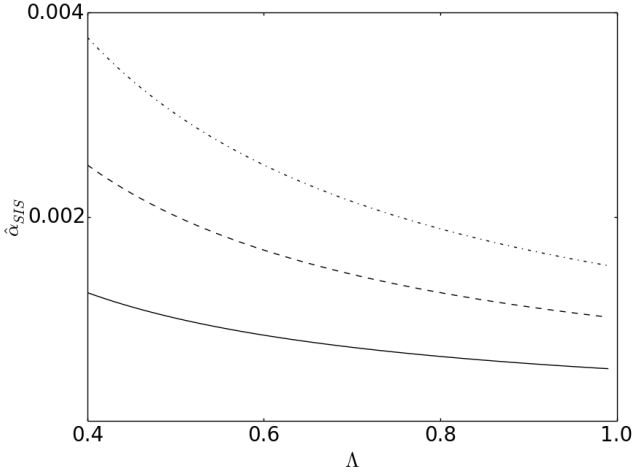


Fig. 6: Plot of $\hat{\alpha}_{SIS}$ vs. Λ for $\tilde{J}_r = 0.1$ (continuous line), $\tilde{J}_r = 0.2$ (dashed line), and $\tilde{J}_r = 0.3$ (dot-dashed line). We used, $\bar{b} = 10$, $\sin \chi = 1$, and $\omega_c^2/\omega^2 = 0.5$.

In Fig. 7, on the other hand, we plot $\hat{\alpha}_{SIS}$ as a function of \tilde{J}_r for different values of Λ . From this figure we conclude that, not only the dragging of the inertial system, but also the boosted parameter Λ contribute to the deflection angle: the greater the values of \tilde{J}_r (plus small values of Λ) the greater the value of the deflection angle $\hat{\alpha}_{SIS}$.

5.2 Non-singular isothermal gas sphere

Now we consider a gravitational lens model for an isothermal sphere. For this model, the singularity at the origin is replaced by a finite core and the density distribution is given in [79]

$$\rho(r) = \frac{\sigma_v^2}{2\pi(r^2 + r_c^2)} = \frac{\rho_0}{\left(1 + \frac{r^2}{r_c^2}\right)}, \quad \rho_0 = \frac{\sigma_v^2}{2\pi r_c^2}, \quad (61)$$

where r_c is the core radius.

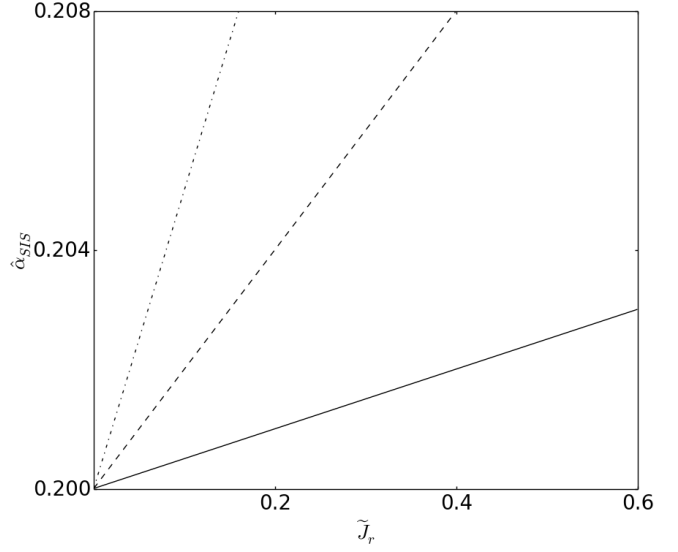


Fig. 7: Plot of $\hat{\alpha}_{SIS}$ vs. \tilde{J}_r for $\Lambda = 1$ (continuous line), $\Lambda = 0.25$ (dashed line), and $\Lambda = 0.1$ (dot-dashed line). We used, $\bar{b} = 10$, $\sin \chi = 1$, and $\omega_c^2/\omega^2 = 0.5$.

Therefore, after substitution of Eq. (61) in Eqs. (57) and (58), the plasma frequency is expressed as

$$\omega_e^2 = \frac{K_e \sigma_v^2}{2\pi \kappa m_p (r^2 + r_c^2)}. \quad (62)$$

Then, from Eqs. (55) and (58), the contributions to the deflection angle are (see Appendix II)

$$\hat{\alpha}_{S2} = \frac{2\bar{b}\omega_c^2}{\pi\omega^2} \left[\frac{1}{4\bar{b}^2\bar{r}_c^2} - \frac{\operatorname{arctanh}\left(\frac{\bar{r}_c}{\sqrt{4\bar{b}^2 + \bar{r}_c^2}}\right)}{\bar{r}_c^3\sqrt{\bar{r}_c^2 + 4\bar{b}^2}} \right], \quad (63)$$

$$\hat{\alpha}_{S3} = -\frac{1}{2} \frac{\bar{b}\omega_c^2}{(4\bar{b}^2 + \bar{r}_c^2)^{3/2}\omega^2}, \quad (64)$$

$$\hat{\alpha}_{B2} = -\frac{\tilde{J}_r\omega_c^2}{2\pi\Lambda\omega^2} \left[\frac{1}{4\bar{b}^2\bar{r}_c^2} - \frac{\operatorname{arctanh}\left(\frac{\bar{r}_c}{\sqrt{4\bar{b}^2 + \bar{r}_c^2}}\right)}{\bar{r}_c^3\sqrt{\bar{r}_c^2 + 4\bar{b}^2}} \right], \quad (65)$$

$$\hat{\alpha}_{B3} = \frac{6}{\pi} \frac{\bar{b}^2\tilde{J}_r\omega_c^2}{\Lambda\omega^2} \left[\frac{2\bar{r}_c^2 - 12\bar{b}^2}{48\bar{b}^4\bar{r}_c^4} + \frac{\operatorname{arctanh}\left(\frac{\bar{r}_c}{\sqrt{4\bar{b}^2 + \bar{r}_c^2}}\right)}{\bar{r}_c^5\sqrt{\bar{r}_c^2 + 4\bar{b}^2}} \right], \quad (66)$$

where $\omega_c^2 = \frac{K_e \sigma_v^2}{M^2 \kappa m_p}$, $\bar{r}_c = r_c/M$, $\tilde{J}_r = J_r/M^2$, and $\bar{b} = b/2M$.

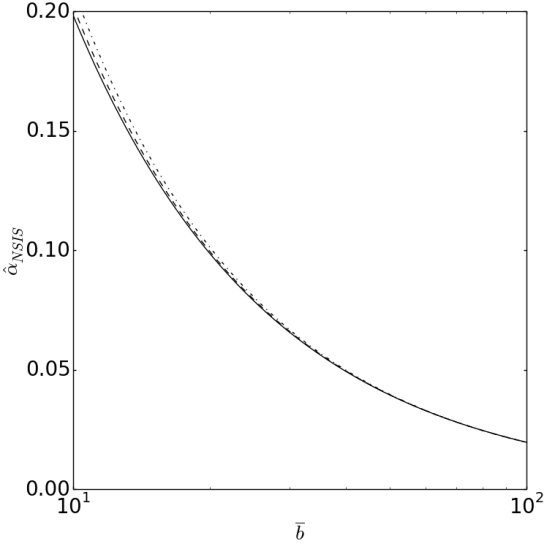


Fig. 8: Plot of $\hat{\alpha}_{NSIS}$ vs. \bar{b} for $\Lambda = 1$ (continuous line), $\Lambda = 0.25$ (dashed line), and $\Lambda = 0.1$ (dot-dashed line). We used, $\tilde{J}_r = 0.25$, $\bar{r}_c = 10$, $\sin \chi = 1$, and $\omega_c^2/\omega^2 = 0.5$.

In Fig. 8 we plot $\hat{\alpha}_{NSIS}$ as a function of \bar{b} for different values of Λ . In the plot, we have $\bar{b} \gg \bar{r}_c$ because we are in the weak field limit. According to the figure, the behavior is quite similar to that of the deflection angle in the case of a singular plasma distribution: there are small differences in $\hat{\alpha}_{NSIS}$ when small values of Λ are considered, and no there is no difference in the deflection angle when the impact parameter \bar{b} takes values greater than 10. Fig. 9 helps to see this behavior clearly.

In Fig. 10 we plot the deflection angle as a function of \tilde{J}_r for different values of Λ . Once again, the dragging of the inertial system along with small values of the boosted parameter Λ play an important role when compared with the slowly rotating case [25].

5.3 Plasma in a galaxy cluster

In a galaxy cluster, due to the large temperature of the electrons, the distribution of electrons may be homogeneous. Therefore, it is proper to suppose a singular isothermal sphere as a model for the distribution of the gravitating matter. Using this approximation, and without considering the mass of the plasma, Bisnovaty-Kogan and O. Yu. Tsupko solved the equation of hydrostatic equilibrium of a plasma in a gravitational field finding that the plasma density distribution has the

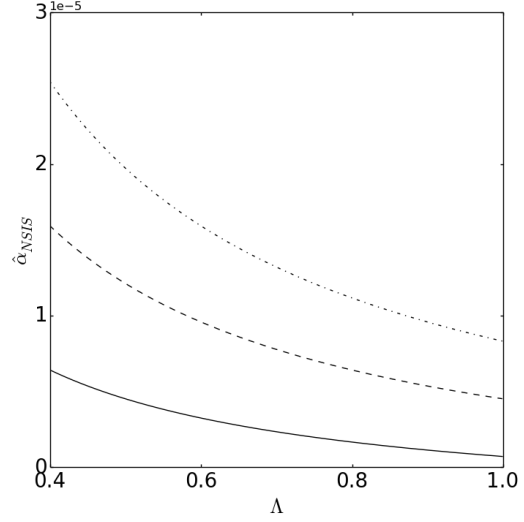


Fig. 9: Plot of $\hat{\alpha}_{NSIS}$ vs. Λ for $\tilde{J}_r = 0.1$ (continuous line), $\tilde{J}_r = 0.2$ (dashed line), and $\tilde{J}_r = 0.3$ (dot-dashed line). We used, $\bar{b} = 100$, $\bar{r}_c = 10$, $\sin \chi = 1$, and $\omega_c^2/\omega^2 = 0.5$. Note the scale used for the deflection angle: each value is multiplied by $1e - 5 = 1 \times 10^{-5}$

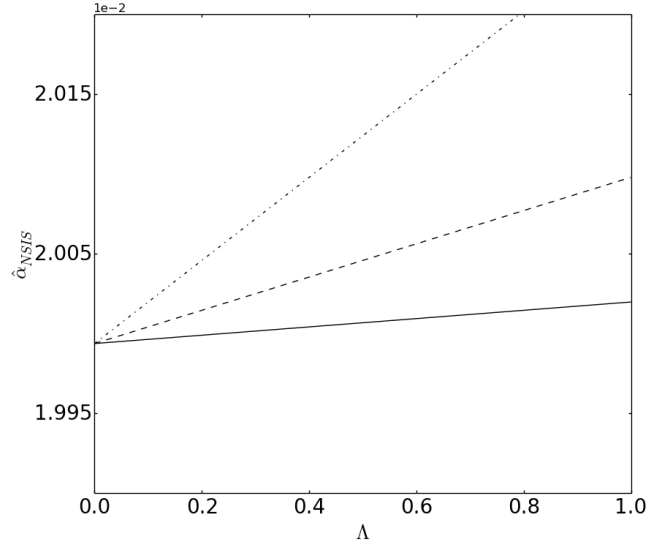


Fig. 10: Plot of $\hat{\alpha}_{NSIS}$ vs. \tilde{J}_r for $\Lambda = 1$ (continuous line), $\Lambda = 0.25$ (dashed line), and $\Lambda = 0.1$ (dot-dashed line). We used, $\bar{b} = 100$, $\bar{r}_c = 10$, $\sin \chi = 1$, and $\omega_c^2/\omega^2 = 0.5$. Note the scale used for the deflection angle: each value is multiplied by $1e - 2 = 1 \times 10^{-2}$

form [22].

$$\rho(r) = \rho_0 \left(\frac{r}{r_0} \right)^{-s}, s = \frac{2\sigma_v^2}{\Re T}, \quad (67)$$

and the plasma frequency is equal to

$$\omega_e^2 = \frac{\rho_0 K_e}{\kappa m_p} \left(\frac{r}{r_0} \right)^{-s}. \quad (68)$$

Hence, using Eqs. (55) and (58) once again, the contributions to the deflection angle are (see Appendix II)

$$\hat{\alpha}_{S2} = \frac{\sqrt{\pi}}{2^{s+1}(s+1)} \frac{\bar{r}_0^s \omega_f^2}{\bar{b}^2 \omega^2} \frac{\Gamma(\frac{s}{2} + 1)}{\Gamma(\frac{s+1}{2})}, \quad (69)$$

$$\hat{\alpha}_{S3} = -\frac{\sqrt{\pi}}{2^s} \frac{\omega_f^2}{\omega^2} \frac{\Gamma(\frac{s}{2} + 1)}{\Gamma(\frac{s}{2})} \left(\frac{\bar{r}_0}{\bar{b}} \right)^s, \quad (70)$$

$$\hat{\alpha}_{B2} = -\frac{\pi}{2^{s+2}(s+1)} \frac{\tilde{J}_r \bar{r}_0^2 \omega_f^2}{\bar{b}^{s+2} \Lambda \omega^2} \frac{\Gamma(\frac{s}{2} + 1)}{\Gamma(\frac{s+1}{2})}, \quad (71)$$

$$\hat{\alpha}_{B3} = \frac{3\sqrt{\pi}}{2^{s+2}(s+3)} \frac{\tilde{J}_r \bar{r}_0^s \omega_f^2}{\bar{b}^{s+2} \Lambda \omega^2} \frac{\Gamma(\frac{s+4}{2})}{\Gamma(\frac{s+1}{2})}, \quad (72)$$

where $\omega_f^2 = \frac{K_e \rho_0}{\kappa m_p}$, $\bar{r}_0 = r_0/M$, $\tilde{J}_r = J_r/M^2$, and $\bar{b} = b/2M$.

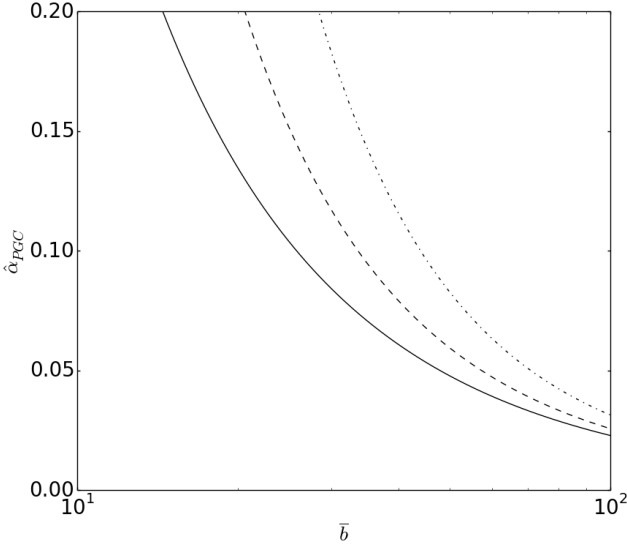


Fig. 11: Plot of $\hat{\alpha}_{PGC}$ vs. \bar{b} for $\Lambda = 1$ (continuous line), $\Lambda = 0.25$ (dashed line), and $\Lambda = 0.1$ (dot-dashed line). We used, $\tilde{J}_r = 0.25$, $\bar{r}_0 = 10$, $\sin \chi = 1$, $s = 0.03$, and $\omega_f^2/\omega^2 = 0.5$.

In Figs. 11, 12, and 13 we plot $\hat{\alpha}_{PGC}$ as a function of \bar{b} , Λ , and \tilde{J}_r , respectively. In order to obtain these plots we considered the case $s \ll 1$ [22]. According to Figs. 11 and 12, differences in the deflection angle can be seen clearly for the **PGC** distribution when compared with the previous distributions. Furthermore,

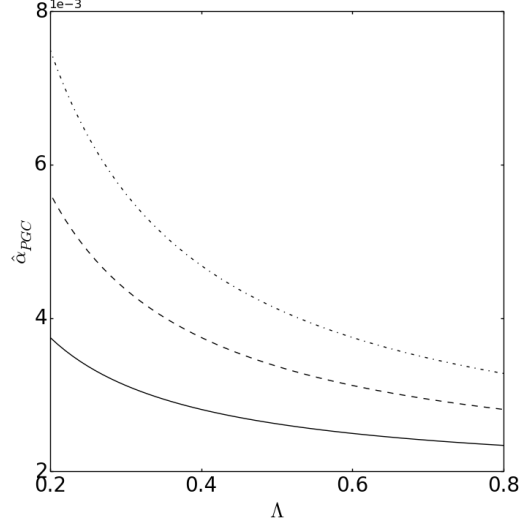


Fig. 12: Plot of $\hat{\alpha}_{PGC}$ vs. Λ for $\tilde{J}_r = 0.1$ (continuous line), $\tilde{J}_r = 0.2$ (dashed line), and $\tilde{J}_r = 0.3$ (dot-dashed line). We used $\bar{r}_0 = 10$, $\sin \chi = 1$, $s = 0.03$, $\bar{b} = 100$ and $\omega_f^2/\omega^2 = 0.5$. Note the scale used for the deflection angle: each value is multiplied by $1e-3 = 1 \times 10^{-3}$.

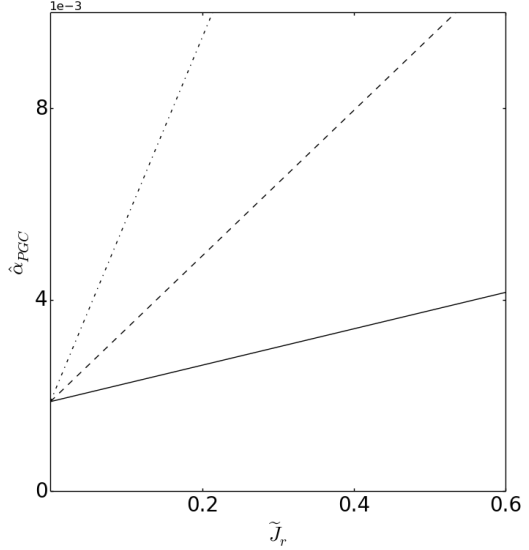


Fig. 13: Plot of $\hat{\alpha}_{PGC}$ vs. \tilde{J}_r for $\Lambda = 1$ (continuous line), $\Lambda = 0.25$ (dashed line), and $\Lambda = 0.1$ (dot-dashed line). We used $\bar{r}_0 = 1.2$, $\sin \chi = 1$, $s = 0.03$, $\bar{b} = 100$ and $\omega_f^2/\omega^2 = 0.5$. Note the scale used for the deflection angle: each value is multiplied by $1e-3 = 1 \times 10^{-3}$.

Fig. 13 shows that the deflection angle increases due to the dragging and small values of Λ .

On the other hand, in Fig. 14, we plotted the behavior of the deflection angle for all distributions as a function of the impact parameter \bar{b} . Note that the values of $\hat{\alpha}$ for the **PGC** distribution are greater than the other two distributions. In the figure there is a small difference between **SIS** and **NSIS** distributions for small values of $b/2M$.

Finally, in Fig. 15 we plotted $\hat{\alpha}$ as a function of ω_c^2/ω^2 (for **SIS** and **NSIS**) and ω_f^2/ω^2 (for **PGC**). This figure clearly show that the deflection angle is more affected by the plasma for the **PGC** distribution than the other two for values of ω_f^2/ω^2 greater than 0.4.

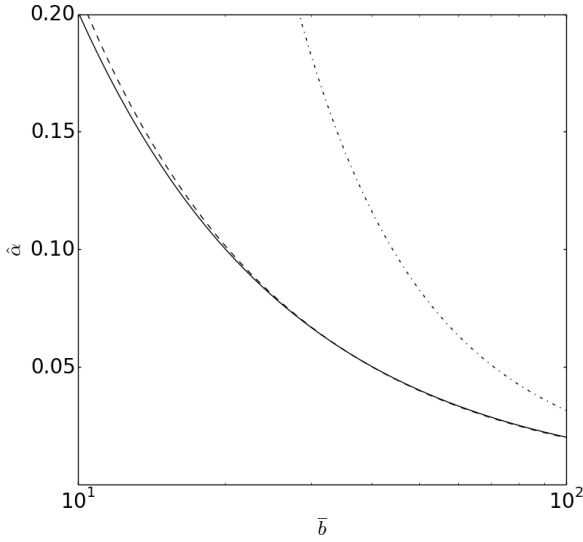


Fig. 14: Plot of $\hat{\alpha}$ vs. \bar{b} for **SIS** (continuous line), **NSIS** (dashed line), and **PGC** (dot-dashed line). We used $\Lambda = 0.1$, $\bar{r}_c = 10$, $\bar{r}_0 = 10$, $\sin \chi = 1$, $s = 0.03$, and $\omega_f^2/\omega^2 = \omega_c^2/\omega^2 = 0.5$. For **NSIS** we use $\Lambda = 1$ since no difference from **SIS** was found.

6 Lens equation and magnification in the presence of plasma

In this section, we compute the magnification for the boosted Kerr metric in the presence of plasma. We consider the uniform and the **SIS** plasma distributions discussed previously in sections 4.2 and 5 respectively.

The magnification of brightness of the star is defined by the relation[25]

$$\mu_\Sigma = \frac{I_{tot}}{I_*} = \sum_k \left| \left(\frac{\theta_k}{\beta} \right) \left(\frac{d\theta_k}{d\beta} \right) \right|, \quad k = 1, 2, \dots, m, \quad (73)$$

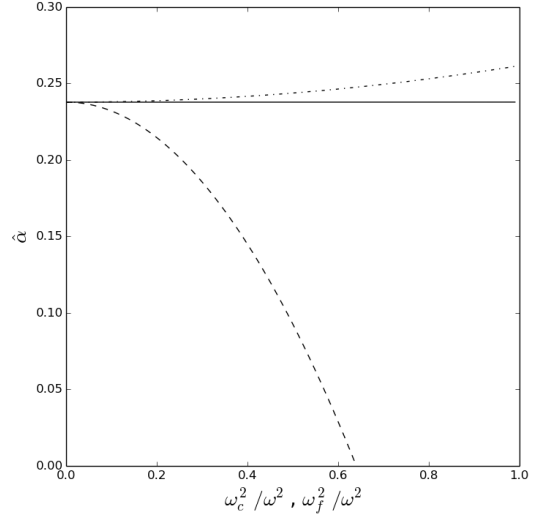


Fig. 15: Plot of $\hat{\alpha}$ vs. ω_f^2/ω^2 , ω_c^2/ω^2 for **SIS** (continuous line), **NSIS** (dashed line), and **PGC** (dot-dashed line). We used $\Lambda = 0.1$, $\bar{r}_c = 10$, $\bar{r}_0 = 10$, $\sin \chi = 1$, $s = 0.03$, and $\bar{b} = 9$

where m is the number of images, I_{tot} is the total brightness of the images, I_* is the unlensed brightness of the source, θ_k is the position of the image, and β is the angular position of the source (see figure 2). In this sense, in order to compute the contribution of the boosted parameter Λ to magnification, we have to solve the lens equation; which is given by the relation[25]

$$\theta D_s = \beta D_s + \hat{\alpha} D_{ls}, \quad (74)$$

here D_s is the distance from the observer to the source, D_{ls} is the distance from the lens to the source, $\hat{\alpha}$ is the deflection angle, and θ , β the positions of the image and the source respectively (see figure 2).

6.1 Uniform plasma

In the case of small angles, it is well known that the impact parameter can be expressed as

$$b \approx D_l \theta, \quad (75)$$

where D_l is the distance from the observer to the lens. Therefore, after using equation (53), the lens equation for the slowly rotating case in the presence of uniform plasma takes the form

$$\theta^3 - \beta \theta^2 - \frac{\theta_E^2}{2} \left(1 + \frac{1}{1 - \frac{\omega_e^2}{\omega^2}} \right) \theta - \frac{\theta_E^2 \tilde{J}_r}{4 \bar{D}_l \Lambda} \frac{1}{\sqrt{1 - \frac{\omega_e^2}{\omega^2}}} = 0. \quad (76)$$

In the last expression, in order to be consistent with the notation, we use $\bar{b} \approx \bar{D}_l \theta$, where $\bar{D}_l = D_l/2M$. Furthermore, we have defined

$$\theta_E^2 = \frac{4MD_{ls}}{D_l D_s} = \frac{2\bar{D}_{ls}}{\bar{D}_l \bar{D}_s}, \quad (77)$$

with $\bar{D}_{ls} = D_{ls}/2M$ and $\bar{D}_s = D_s/2M$. θ_E is known as the Einstein angle. Note that equation (76) reduces to that obtained by [25] for $\Lambda = 1$ ($v = 0$).

In order to solve equation (76) we introduce a new variable x by the relation (see [25, 80] for details.)

$$\theta = x + \frac{\beta}{3}; \quad (78)$$

form which equation (76) reduces to

$$x^3 + px + q = 0, \quad (79)$$

where

$$p = -\frac{\beta^2}{3} - \frac{\theta_E^2}{2} \left(1 + \frac{1}{1 - \frac{\omega_E^2}{\omega^2}}\right) \\ q = -\frac{2\beta^3}{27} - \frac{\beta\theta_E^2}{6} \left(1 + \frac{1}{1 - \frac{\omega_E^2}{\omega^2}}\right) - \frac{\theta_E^2 \tilde{J}_r}{4\bar{D}_l \Lambda} \frac{1}{\sqrt{1 - \frac{\omega_E^2}{\omega^2}}}. \quad (80)$$

Note that the variable q , in contrast with the result obtained by [25], depends on the boosted parameter Λ .

Equation (79) has three different real roots if

$$\frac{q^2}{4} + \frac{p^3}{27} < 0. \quad (81)$$

Therefore, the solution has the form

$$x = 2\sqrt[3]{r} \cos \frac{\phi + 2k\pi}{3}, \quad k = 0, 1, 2 \quad (82)$$

with

$$r = \sqrt{-\frac{p^3}{27}}, \quad \cos \phi = -\frac{q}{2r}. \quad (83)$$

Hence, after using equations (73) and (78), we obtain

$$\mu_{\Sigma tot} = \sum_k \left| \frac{\theta_k}{\beta} \frac{d\theta_k}{d\beta} \right| = \sum_k \left| \frac{x_k + \beta/3}{\beta} \left(\frac{dx_k}{d\beta} + \frac{1}{3} \right) \right| \\ = \sum_k \left| \frac{1}{3\beta} \left(2\sqrt[3]{r} \cos \frac{\phi + 2k\pi}{3} + \frac{\beta}{3} \right) \right| \\ \times \left| \left[\frac{2r\beta}{\sqrt[3]{r^2}} \cos \frac{\phi + 2k\pi}{3} - 2\sqrt[3]{r} \phi_\beta \sin \frac{\phi + 2k\pi}{3} + 1 \right] \right| \quad (84)$$

for $k = 0, 1, 2$. The subscript β denotes the derivatives of the corresponding variables with respect to β .

In reference [81] the authors found that the magnification for small values of β has the form (see equation (32) in [25])

$$\mu = \frac{1}{2} \frac{\sqrt{2\theta_E^2 \left(1 + \frac{1}{1 - \frac{\omega_E^2}{\omega^2}}\right)}}{\beta}. \quad (85)$$

Therefore, in order to study the behaviour of the magnification for small values of β , and compare with the case of uniform plasma studied by Bisnovatyi-Kogan and Tsupko (2010), it is necessary to express equation (84) in the limit $\beta \rightarrow 0$. Hence, for small values of β we have that

$$\sqrt[3]{r} \rightarrow \sqrt{\frac{1}{6} \theta_E^2 \left(1 + \frac{1}{1 - \frac{\omega_E^2}{\omega^2}}\right)}, \\ r_\beta \rightarrow 0, \\ \phi_\beta \rightarrow \frac{1}{\sqrt{1 - \left(\frac{q}{2r}\right)^2}} \frac{q_\beta}{2r} \\ q_\beta \rightarrow -\frac{\beta\theta_E^2}{6} \left(1 + \frac{1}{1 - \frac{\omega_E^2}{\omega^2}}\right) \\ \cos \phi = -\frac{q}{2r} \rightarrow \frac{\sqrt{27}}{\sqrt{2}} \frac{1}{\theta_E} \frac{\tilde{J}_r}{\bar{D}_l \Lambda} \frac{1}{\sqrt{1 - \frac{\omega_E^2}{\omega^2}}} \frac{1}{\sqrt{\left(1 + \frac{1}{1 - \frac{\omega_E^2}{\omega^2}}\right)^3}}. \quad (86)$$

Where we have followed the same analysis done in [25]. Note that $-q/2r$, in our case, depends on Λ . Thus, after using equations (84), (85), and (86), we found that $\mu_{\Sigma tot}/\mu$, in the limit $\beta \rightarrow 0$, takes the form

$$\frac{\mu_{\Sigma tot}}{\mu} = \frac{1}{3\sqrt{3}} \sum_k \left| \frac{\sin \frac{2(\phi + 2k\pi)}{3}}{\sqrt{1 - \left(\frac{q}{2r}\right)^2}} + 2 \cos \frac{\phi + 2k\pi}{3} \right|. \quad (87)$$

Now, setting $\tilde{J}_r = 0$ and $\Lambda = 1$, the last expression reduces to

$$\frac{\mu_{\Sigma tot}}{\mu} = \frac{1}{3\sqrt{3}} \sum_k \left| \sin \frac{(1 + 4k)\pi}{3} + 2 \cos \frac{(1 + 4k)\pi}{6} \right| \\ = \frac{1}{3\sqrt{3}} \left| 2 \cos \left(\frac{\pi}{6}\right) + \sin \left(\frac{\pi}{3}\right) \right| \\ + \frac{1}{3\sqrt{3}} \left| 2 \cos \left(\frac{5\pi}{6}\right) + \sin \left(\frac{5\pi}{3}\right) \right| \\ + \frac{1}{3\sqrt{3}} \left| 2 \cos \left(\frac{9\pi}{6}\right) + \sin(3\pi) \right| = 1.$$

(88)

With this result, we have shown that the ratio $\mu_{\Sigma tot}/\mu$ is equal to unity when $\tilde{J}_r = 0$ and $\Lambda = 1$; this means that equation (84) reduces to equation (85) in the limit $\beta \rightarrow 0$.

In Figs. 16.a and 16.c, we plotted the behaviour of the total magnification as a function of the boosted parameter Λ for $\beta = 0.001$ and $\beta = 0.0001$ respectively. According to Fig. 16.a, when $\beta = 0.001$, the total magnification decreases as Λ increases. This means that $\mu_{\Sigma tot}$ decreases as the boosted velocity v of the black hole decreases. A similar behaviour can be seen from Fig. 16.c when $\beta = 0.0001$. Note that for small values of β , the magnitude of the total magnification increases. For example: when $\beta = 0.001$ the total magnification is about $\mu_{\Sigma tot} \approx 52.2$. However, when $\beta = 0.0001$, the value increases to $\mu_{\Sigma tot} \approx 522.2$.

6.2 Singular isothermal sphere

In a similar way, in order to compute the magnification for **SIS**, we also use the approximation of small angles described in equation (75). Hence, after using equation (60), the lens equation for **SIS** takes the form

$$\theta^3 - \beta\theta^2 - \frac{2D_{ls}}{D_l D_s}\theta - \frac{\bar{D}_{ls}}{D_l^2 \bar{D}_s}\left(\frac{\tilde{J}_r}{2\Lambda} - \frac{\omega_c^2}{16\omega^2}\right) = 0 \quad (89)$$

In the last equation, as an approximation, we neglected the second and the last two terms of equation (60) since they are very small in the weak field limit. Then, using equation (77), equation (89) can be expressed in terms of the Einstein angle as:

$$\theta^3 - \beta\theta^2 - \theta_E^2\theta - \frac{\delta\theta_E^2}{\Lambda} = 0, \quad (90)$$

where we defined:

$$\delta = \frac{1}{\bar{D}_l}\left(\frac{\tilde{J}_r}{4} - \frac{\omega_c^2 \Lambda}{32\omega^2}\right). \quad (91)$$

Now, introducing the new variable $y = \theta + \beta/3$, the equation (90) reduces to

$$y^3 + my + n = 0 \quad (92)$$

with,

$$\begin{aligned} m &= -\frac{\beta^2}{3} - \theta_E^2 \\ n &= -\frac{2\beta^3}{27} - \frac{\beta\theta_E^2}{3} - \frac{\delta\theta_E^2}{\Lambda}. \end{aligned} \quad (93)$$

Equation (90) has three different real roots if

$$\frac{m^2}{4} + \frac{n^3}{27} < 0. \quad (94)$$

This condition is already satisfied in our case. Hence the solutions has the form

$$y = 2\sqrt[3]{l} \cos \frac{\epsilon + 2k\pi}{3}, \quad k = 0, 1, 2 \quad (95)$$

with

$$l = \sqrt{-\frac{m^3}{27}}, \quad \cos \epsilon = -\frac{n}{2l} \quad (96)$$

Therefore, after using equations (73) and the new variable y , we obtain

$$\begin{aligned} \mu_\Sigma &= \sum_k \left| \frac{1}{3\beta} \left(2\sqrt[3]{l} \cos \frac{\epsilon + 2k\pi}{3} + \frac{\beta}{3} \right) \right| \\ &\times \left| \left[\frac{2l_\beta}{\sqrt[3]{l^2}} \cos \frac{\epsilon + 2k\pi}{3} - 2\sqrt[3]{l} \epsilon_\beta \sin \frac{\epsilon + 2k\pi}{3} + 1 \right] \right| \end{aligned} \quad (97)$$

for $k = 0, 1, 2$. The subscript β has the same meaning as in equation (84).

In Figs. 16.b and 16.d, we plotted the behaviour of $\mu_{\Sigma tot}$ as a function of the boosted parameter Λ for $\beta = 0.001$ and $\beta = 0.0001$ respectively. In contrast with the previous case (uniform plasma), we see that the total magnification increases as Λ increases. On the other hand, note that for small values of β , the magnitude of $\mu_{\Sigma tot}$ increases: it changes, for example, from 42.6 to 426.3 when β changes from 0.001 to 0.0001 respectively.

7 Conclusion

In this work we have studied the deflection angle for the boosted Kerr metric in the presence of both homogeneous and non-homogeneous plasma, and in the latter case three different distributions have been considered.

In Subsection 4.1 we investigated the behavior of the deflection angle for the non-rotating case in the presence of uniform plasma ($\omega_e = \text{constant}$) by considering small values of v . According to Eq. (46) we found that $\hat{\alpha}_b$ does not depend, at least at first order, on the velocity v . It was also found that, after the approximation $1 - n \ll \frac{\omega_e}{\omega}$, the deflection angle in Eq. (45) reduces to that obtained in [22] (see Eq. (46)). As a consequence, the optics for the non-rotating boosted Kerr metric is the same as Schwarzschild. In this sense, the bending of light, due to the presence of a uniform plasma, is

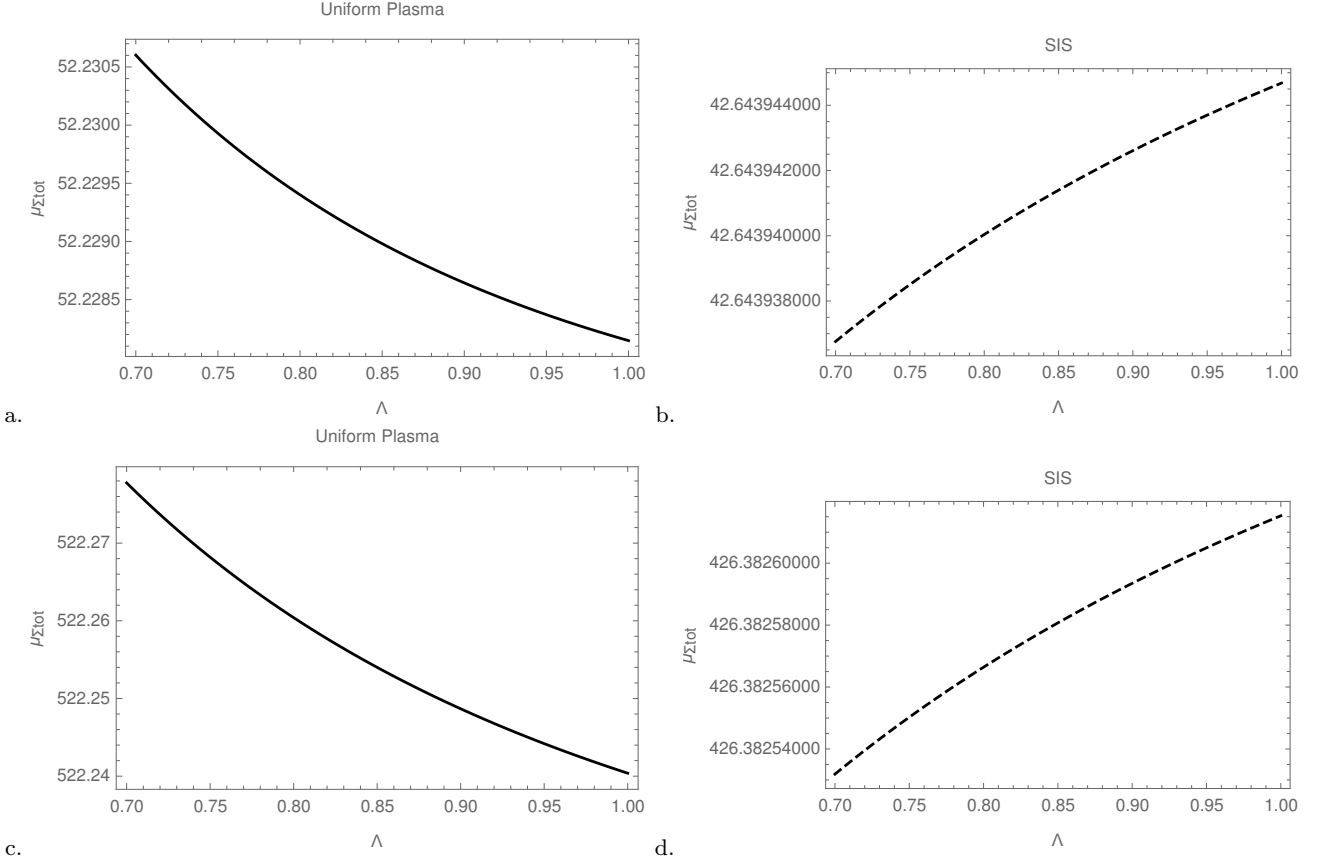


Fig. 16: (a) Plot of $\mu_{\Sigma_{tot}}$ vs. Λ when $\beta = 0.001$ for uniform plasma. (b) Plot of $\mu_{\Sigma_{tot}}$ vs. Λ when $\beta = 0.001$ for the **SIS** distribution. (c) Plot of $\mu_{\Sigma_{tot}}$ vs. Λ when $\beta = 0.0001$ for uniform plasma. (d) Plot of $\mu_{\Sigma_{tot}}$ vs. Λ when $\beta = 0.0001$ for the **SIS** distribution. In all the figures we considered $\bar{D}_{ls} = 10$, $\bar{D}_l = 100$, $\bar{D}_s = 110$, $\omega_e^2/\omega^2 = \omega_c^2/\omega^2 = 0.5$, $\theta_E = 0.001818$, and $\tilde{J}_r = 0.3$.

greater than the Schwarzschild case in vacuum for values of ω_e^2/ω^2 smaller than unity.

In Subsection 4.2, we studied the rotating case by considering a uniform distribution. Following the ideas of [25], we found that the expression for the deflection angle $\hat{\alpha}_b$ in Eq. (53) contains two terms: the Schwarzschild angle $\hat{\alpha}_{bS}$, and the contribution due to the dragging of the inertial frame $\hat{\alpha}_{bD}$. The result is quite similar to that of V.S Morozova et al.. However, in contrast with their result, Eq. (53) also depends on the parameter Λ . This dependence is shown in Fig. 4. From this figure we found that the smaller the values of Λ (constrained to the interval $0 < \Lambda \leq 1$) the greater is the deflection angle. In this sense, not only the dragging and the presence of a plasma, but also the motion of the black hole will contribute to the lensing. Therefore, since no effect was found in the previous case, we may conclude that $\hat{\alpha}_b$ depends on v only when the dragging of the inertial

frame takes place.

In Section 5, we consider the deflection angle in terms of \bar{b} , Λ , and \tilde{J}_r for different distributions. As shown in our figures, $\hat{\alpha}$ is affected by the presence of plasma and is greater when compared with vacuum and uniform distributions. Furthermore, we found again that $\hat{\alpha}$ increases not only due to the dragging, but also when small values of the boosted parameter Λ are considered.

In this work, we also found some important constraints for two of the models. In the case of **NSIS**, for example, the radius of the core r_c must have values greater than $6M$. If the core radius is smaller than this limit the deflection angle becomes negative at some point and will not agree with the usual behavior when $b \rightarrow \infty$. On the other hand, regarding the **PGC**, we found that s must be different from -1 or -3 as can be seen from Eq. (69). Nevertheless, this condition is

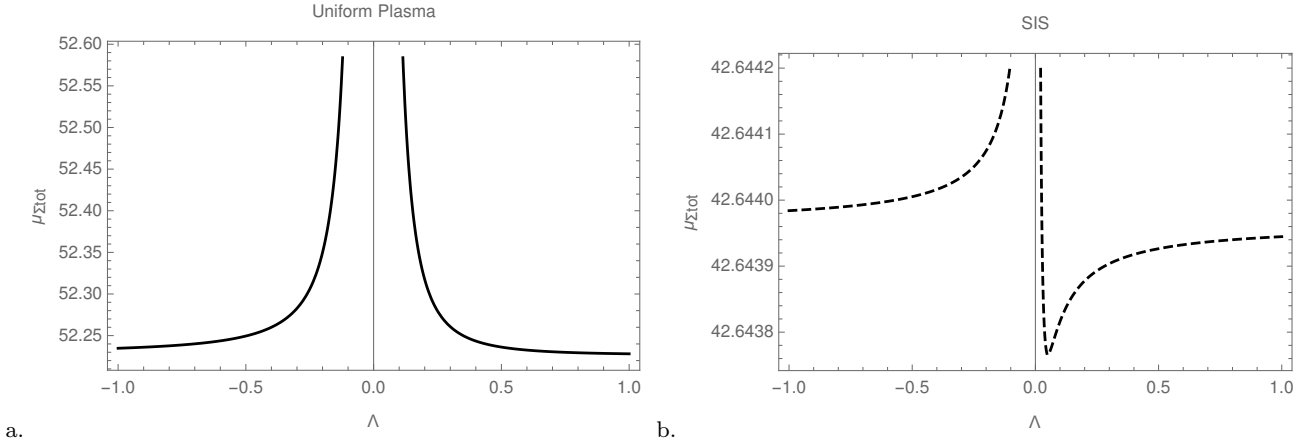


Fig. 17: (a) Plot of $\mu_{\Sigma tot}$ vs. Δ when $\beta = 0.001$ for uniform plasma. (b) Plot of $\mu_{\Sigma tot}$ vs. Δ when $\beta = 0.001$ for the **SIS** distribution. In all the figures we considered $\bar{D}_{ls} = 10$, $\bar{D}_l = 100$, $\bar{D}_s = 110$, $\omega_e^2/\omega^2 = \omega_c^2/\omega^2 = 0.5$, $\theta_E = 0.001818$, and $\tilde{J}_r = 0.3$.

fulfilled since we consider positive values of $s \ll 1$.

No important difference between the models was found when the deflection angle was considered. In the case of **SIS** and **NSIS**, for example, the behavior was very similar. Therefore, under the weak field approximation, it is not possible to distinguish these two distributions. Nevertheless, the deflection angle is affected considerably when we consider a plasma in a galaxy cluster. The values of the deflection angle are greater than those obtained with the other two models. This behavior is clearly shown in Fig. 14. Furthermore, according to Fig. 15, we found that the deflection angle is affected by the plasma when the **PGC** distribution is considered.

Finally, in section 6, as an application, we compute the total magnification for uniform and **SIS** plasma distributions. According to Fig. 16 we conclude that, for small values of v ($0.7 \leq \Delta \leq 1$), the total magnification is greater when the uniform plasma distribution is considered. For example, in the case of uniform distribution (considering $\beta = 0.001$), we see that $\mu_{\Sigma tot} \approx 52.22$. Nevertheless, for the **SIS** distribution, we found that $\mu_{\Sigma tot} \approx 42.64$. A similar behaviour occurs when $\beta = 0.0001$. Furthermore, it is important to point out that the total magnification has small changes in both distributions: $\mu_{\Sigma tot}$ ranges from 52.2285 to 52.2305 for the uniform plasma, and from 42.643938 to 42.643944 in the **SIS**. The change is very small for the last distribution.

On the other hand, when we compare both models (uniform and **SIS** plasma distributions), we see that the

behaviour of the total magnification is different (see figures 17.a and 17.b). In the case of the uniform plasma distribution, for example, when the boosted Kerr Black hole is moving towards ($\Delta > 0$) or away ($\Delta < 0$) from the observer the behaviour is very similar (there is a small difference when $\Delta \rightarrow -1$ and $\Delta \rightarrow 1$). However, when we consider the **SIS** distribution, the behaviour is not symmetric. This behaviour is due to cinematic effects. In this sense, when the magnification is considered, it would be possible to distinguish both models.

Acknowledgements Authors thank the anonymous Referees for carefully reading the manuscript and for their value suggestions. We also want to thank Prof. N. Dadhich for value discussion. This work was supported by the National Natural Science Foundation of China (Grant No. U1531117) and Fudan University (Grant No. IDH1512060). C.A.B.G. also acknowledges support from the China Scholarship Council (CSC), Grant No. 2017GXZ019022. C.B. also acknowledges the support from the Alexander von Humboldt Foundation. The research is supported in part by Grant No. VA-FA-F-2-008 and No.YFA-Ftech-2018-8 of the Uzbekistan Ministry for Innovation Development, by the Abdus Salam International Centre for Theoretical Physics through Grant No. OEA-NT-01 and by Erasmus+ exchange grant between Silesian University in Opava and National University of Uzbekistan.

Appendix I: Transformation to cartesian coordinates

The transformation relations for the non rotating case ($a = 0$) are (see [73])

$$\begin{aligned}\bar{t} &= t \\ \bar{x} &= r \sin \theta \cos \phi \\ \bar{y} &= r \sin \theta \sin \phi \\ \bar{z} &= r \cos \theta.\end{aligned}\quad (98)$$

Therefore, the Jacobian matrix has the form

$$\mathbf{J} = \begin{pmatrix} 1 & 0 & 0 & 0 \\ 0 & \cos \phi \sin \theta & r \cos \phi \cos \theta & -r \sin \phi \sin \theta \\ 0 & \sin \phi \sin \theta & r \sin \phi \cos \theta & r \cos \phi \sin \theta \\ 0 & \cos \theta & -r \sin \theta & 0 \end{pmatrix}. \quad (99)$$

We are seeking for expressions of the form

$$dx^\mu = \frac{\partial x^\mu}{\partial \bar{x}^\nu} d\bar{x}^\nu. \quad (100)$$

In the last expression, x^μ denotes the Boyer-Lindquist coordinates (t, r, θ, ϕ) and \bar{x}^ν denotes the Cartesian coordinates $(\bar{t}, \bar{x}, \bar{y}, \bar{z})$. According to Eq. (100), the Jacobian for the inverse transformation has the form

$$\mathbf{J}^{-1} = \left(\frac{\partial x^\mu}{\partial \bar{x}^\nu} \right). \quad (101)$$

In order to find $\bar{\mathbf{J}}$, we use the well known relation (see [82, 83].)

$$\mathbf{J} \times \mathbf{J}^{-1} = \mathbf{I}. \quad (102)$$

Thus, the inverse transformation is

$$\mathbf{J}^{-1} = \begin{pmatrix} 1 & 0 & 0 & 0 \\ 0 & \cos \phi \sin \theta & \sin \phi \sin \theta & \cos \theta \\ 0 & \frac{\cos \phi \cos \theta}{r} & \frac{\sin \phi \cos \theta}{r} & -\frac{\sin \theta}{r} \\ 0 & -\frac{\sin \phi}{r \sin \theta} & \frac{\cos \phi}{r \sin \theta} & 0 \end{pmatrix}, \quad (103)$$

and,

$$\begin{aligned}dt &= d\bar{t} \\ dr &= \cos \phi \sin \theta d\bar{x} + \sin \phi \sin \theta d\bar{y} + \cos \theta d\bar{z} \\ d\theta &= \frac{\cos \phi \cos \theta}{r} d\bar{x} + \frac{\sin \phi \cos \theta}{r} d\bar{y} - \frac{\sin \theta}{r} d\bar{z} \\ d\phi &= -\frac{\sin \phi}{r \sin \theta} d\bar{x} + \frac{\cos \phi}{r \sin \theta} d\bar{y}.\end{aligned}\quad (104)$$

Then, after substitution in Eq. (38) and taking into account that $dt = d\bar{t}$, the line element reduces to equation

$$\begin{aligned}ds^2 &= ds_0^2 + h_{11} d\bar{x}^2 + h_{12} d\bar{x} d\bar{y} + h_{13} d\bar{x} d\bar{z} \\ &\quad + h_{22} d\bar{y}^2 + h_{23} d\bar{y} d\bar{z} + \underbrace{\frac{2M}{r} dt^2}_{h_{00}} \\ &\quad + \underbrace{d\bar{z}^2 \left(\frac{2M}{r} \cos^2 \theta - 2v \cos \theta \sin^2 \theta \right)}_{h_{33}},\end{aligned}\quad (105)$$

where

$$\begin{aligned}h_{11} &= -2v(\cos^2 \phi \cos^3 \theta + \sin^2 \phi \cos \theta) \\ h_{12} &= 4v(2 \cos \phi \sin \phi \cos \theta - \cos \phi \sin \phi \cos^3 \theta) \\ h_{13} &= 4 \left(\frac{M \cos \phi \cos \theta \sin \theta}{r} + v \cos \phi \cos^2 \theta \sin \theta \right) \\ h_{22} &= 2 \left[\frac{M \sin^2 \phi \sin^2 \theta}{r} - v(\sin^2 \phi \cos^3 \theta + 2 \cos^2 \phi \cos \theta) \right] \\ h_{23} &= 4v \sin \phi \cos^2 \theta \sin \theta\end{aligned}\quad (106)$$

For $v = 0$, the line element in Eq. (105) reduces to the Schwarzschild case obtained in [22].

Appendix II: Plasma distributions integrals

Integrals in uniform plasma non-rotating case:

The first integral in equation (46) is

$$\int_{-\infty}^{\infty} \frac{dz}{(b^2 + z^2)^{\frac{3}{2}}} = 2 \int_0^{\infty} \frac{dz}{(b^2 + z^2)^{\frac{3}{2}}} = \frac{2}{b^2} \quad (107)$$

Integrals in SIS:

From Eqs. (55) and (58) and the well known property of the Γ -function [78]

$$\int_0^{\infty} \frac{dz}{(z^2 + b^2)^{\frac{h}{2}+1}} = \frac{1}{hb^{h+1}} \frac{\sqrt{\pi} \Gamma(\frac{h}{2} + \frac{1}{2})}{\Gamma(\frac{h}{2})}, \quad (108)$$

the integrals of $\hat{\alpha}_{S2}$, $\hat{\alpha}_{S3}$, $\hat{\alpha}_{B2}$ and $\hat{\alpha}_{B3}$ are respectively

$$\begin{aligned}I_{S2} &= \int_0^{\infty} \frac{dz}{(b^2 + z^2)^{\frac{3}{2}+1}} = \frac{\sqrt{\pi}}{3b^4} \frac{\Gamma(2)}{\Gamma(3/2)} = \frac{2}{3b^4} \\ I_{S3} &= \int_0^{\infty} \frac{dz}{(b^2 + z^2)^2} = \frac{\sqrt{\pi}}{2b^3} \frac{\Gamma(3/2)}{\Gamma(1)} = \frac{\pi}{4b^3} \\ I_{B2} &= \int_0^{\infty} \frac{dz}{(b^2 + z^2)^{\frac{3}{2}+1}} = \frac{2}{3b^4} \\ I_{B3} &= \int_0^{\infty} \frac{dz}{(b^2 + z^2)^{\frac{5}{2}+1}} = \frac{\sqrt{\pi}}{5b^6} \frac{\Gamma(3)}{\Gamma(5/2)} = \frac{8}{15b^6}\end{aligned}\quad (109)$$

Integrals in NSIS:

The integrals of $\hat{\alpha}_{S2}$, $\hat{\alpha}_{S3}$, $\hat{\alpha}_{B2}$ and $\hat{\alpha}_{B3}$, after substitution of Eq. (58) in (55), are respectively

$$\begin{aligned}\bar{I}_{S2} &= \int_0^\infty \frac{dz}{(z^2 + b^2 + r_c^2)(b^2 + z^2)^{\frac{3}{2}}} \\ &= \frac{1}{b^2 r_c^2} - \frac{\operatorname{arctanh}\left(\frac{r_c}{\sqrt{b^2 + r_c^2}}\right)}{r_c^3 \sqrt{b^2 + r_c^2}} \\ \bar{I}_{S3} &= - \int_0^\infty \frac{dz}{(z^2 + b^2 + r_c^2)^2} \\ &= - \frac{\sqrt{\pi}}{2(b^2 + r_c^2)^{\frac{3}{2}}} \frac{\Gamma(3/2)}{\Gamma(1)} \\ \bar{I}_{B2} &= \bar{I}_{S2} \\ \bar{I}_{B3} &= \int_0^\infty \frac{dz}{(z^2 + b^2 + r_c^2)(b^2 + z^2)^{\frac{3}{2}}} \\ &= \frac{2r_c^2 - 3b^2}{3r_c^4 b^4} + \frac{\operatorname{arctanh}\left(\frac{r_c}{\sqrt{b^2 + r_c^2}}\right)}{r_c^5 \sqrt{r_c^2 + b^2}}\end{aligned}\quad (110)$$

Integrals in PGC:

The integrals of $\hat{\alpha}_{S2}$, $\hat{\alpha}_{S3}$, $\hat{\alpha}_{B2}$ and $\hat{\alpha}_{B3}$, after substitution of Eq. (58) in (55), are respectively

$$\begin{aligned}\tilde{I}_{S2} &= \int_0^\infty \frac{dz}{(b^2 + z^2)^{\frac{s+1}{2}+1}} = \frac{\sqrt{\pi}}{(s+1)b^{s+2}} \frac{\Gamma(\frac{s}{2}+1)}{\Gamma(\frac{s+1}{2})} \\ \tilde{I}_{S3} &= - \int_0^\infty \frac{dz}{(b^2 + z^2)^{\frac{s}{2}+1}} = \frac{\sqrt{\pi}}{sb^{s+1}} \frac{\Gamma(\frac{s+1}{2})}{\Gamma(\frac{s}{2})} \\ \tilde{I}_{B2} &= \tilde{I}_{S2} \\ \tilde{I}_{B3} &= \int_0^\infty \frac{dz}{(b^2 + z^2)^{\frac{s+3}{2}+1}} = \frac{\sqrt{\pi}}{(s+3)b^{s+4}} \frac{\Gamma(\frac{s+4}{2})}{\Gamma(\frac{s+3}{2})}\end{aligned}\quad (111)$$

References

1. B.P. Abbott, R. Abbott, T.D. Abbott, M.R. Abernathy, F. Acernese, K. Ackley, C. Adams, T. Adams, P. Addesso, R.X. Adhikari, et al., *Physical Review Letters* **116**(22), 221101 (2016). DOI 10.1103/PhysRevLett.116.221101
2. The LIGO Scientific Collaboration, the Virgo Collaboration, The LIGO Scientific Collaboration, the Virgo Collaboration, B.P. Abbott, R. Abbott, T.D. Abbott, M.R. Abernathy, F. Acernese, K. Ackley, et al., *Physical Review Letters* **116**(24), 241102 (2016). DOI 10.1103/PhysRevLett.116.241102
3. B.P. Abbott, R. Abbott, T.D. Abbott, M.R. Abernathy, F. Acernese, K. Ackley, C. Adams, T. Adams, P. Addesso, R.X. Adhikari, et al., *Astrophys. J. Lett.* **833**, L1 (2016). DOI 10.3847/2041-8205/833/1/L1
4. V.S. Morozova, L. Rezzolla, B.J. Ahmedov, *Phys. Rev. D* **89**(10), 104030 (2014). DOI 10.1103/PhysRevD.89.104030
5. M. Lyutikov, *Phys. Rev. D* **83**(6), 064001 (2011). DOI 10.1103/PhysRevD.83.064001
6. I.D. Soares, *General Relativity and Gravitation* **49**, 77 (2017). DOI 10.1007/s10714-017-2239-2
7. J.L. Synge, *Relativity: The General Theory*. (North-Holland, Amsterdam, 1960)
8. P. Schneider, J. Ehlers, E.E. Falco, *Gravitational Lenses, XIV, 560 pp. 112 figs.. Springer-Verlag Berlin Heidelberg New York. Also Astronomy and Astrophysics Library* (1999)
9. V. Perlick, *Ray Optics, Fermat's Principle, and Applications to General Relativity* (Springer-Verlag, 2000)
10. V. Perlick, *Living Reviews in Relativity* **7**, 9 (2004). DOI 10.12942/lrr-2004-9
11. A. Rogers, *Mon. Not. R. Astron. Soc.* **451**, 17 (2015). DOI 10.1093/mnras/stv903
12. A. Rogers, *Universe* **3**, 3 (2017). DOI 10.3390/universe3010003
13. X. Er, A. Rogers, *Mon. Not. R. Astron. Soc.* **475**, 867 (2018). DOI 10.1093/mnras/stx3290
14. A. Rogers, *Mon. Not. R. Astron. Soc.* **465**, 2151 (2017). DOI 10.1093/mnras/stw2829
15. A. Broderick, R. Blandford, *Mon. Not. R. Astron. Soc.* **342**, 1280 (2003). DOI 10.1046/j.1365-8711.2003.06618.x
16. J. Bicak, P. Hadrava, *Astronomy and Astrophysics* **44**, 389 (1975)
17. S. Kichenassamy, R.A. Krikorian, *Phys. Rev. D* **32**, 1866 (1985). DOI 10.1103/PhysRevD.32.1866
18. V. Perlick, O.Y. Tsupko, *Phys. Rev. D* **95**(10), 104003 (2017). DOI 10.1103/PhysRevD.95.104003
19. V. Perlick, O.Y. Tsupko, G.S. Bisnovatyi-Kogan, *Phys. Rev. D* **92**(10), 104031 (2015). DOI 10.1103/PhysRevD.92.104031
20. A. Abdujabbarov, B. Toshmatov, J. Schee, Z. Stuchlík, B. Ahmedov, *International Journal of Modern Physics D* **26**, 1741011-187 (2017). DOI 10.1142/S0218271817410115
21. E.F. Eiroa, C.M. Sendra, *Phys.Rev. D* **86**(8), 083009 (2012). DOI 10.1103/PhysRevD.86.083009
22. G.S. Bisnovatyi-Kogan, O.Y. Tsupko, *Monthly Notices of the Royal Astronomical Society* **404**, 1790 (2010). DOI 10.1111/j.1365-2966.2010.16290.x
23. O.Y. Tsupko, G.S. Bisnovatyi-Kogan, in *American Institute of Physics Conference Series, American Institute of Physics Conference Series*, vol. 1206, ed. by S.K. Chakrabarti, A.I. Zhuk, G.S. Bisnovatyi-Kogan (2010), *American Institute of Physics Conference Series*, vol. 1206, pp. 180–187. DOI 10.1063/1.3292524
24. O.Y. Tsupko, G.S. Bisnovatyi-Kogan, *Gravitation and Cosmology* **18**, 117 (2012). DOI 10.1134/S0202289312020120
25. V.S. Morozova, B.J. Ahmedov, A.A. Tursunov, *Astrophys Space Sci* **346**, 513 (2013). DOI 10.1007/s10509-013-1458-6

26. O.Y. Tsupko, G.S. Bisnovatyi-Kogan, *Gravitation and Cosmology* **20**, 220 (2014). DOI 10.1134/S0202289314030153
27. G. Bisnovatyi-Kogan, O. Tsupko, *Universe* **3**, 57 (2017). DOI 10.3390/universe3030057
28. A. Hakimov, F. Atamurotov, *Astrophys Space Sci* **361**, 112 (2016). DOI 10.1007/s10509-016-2702-7
29. B. Turimov, B. Ahmedov, A. Abdujabbarov, C. Bambi, ArXiv e-prints: gr-qc 1802.03293 (2018)
30. C.A. Benavides, A. Cárdenas-Avendaño, A. Larranaga, *International Journal of Theoretical Physics* **55**(4), 2219 (2016). DOI 10.1007/s10773-015-2861-2. URL <https://doi.org/10.1007/s10773-015-2861-2>
31. G.V. Kraniotis, *General Relativity and Gravitation* **46**, 1818 (2014). DOI 10.1007/s10714-014-1818-8
32. A. de Vries, *Classical and Quantum Gravity* **17**, 123 (2000). DOI 10.1088/0264-9381/17/1/309
33. A. Abdujabbarov, B. Ahmedov, N. Dadhich, F. Atamurotov, *Phys. Rev. D* **96**(8), 084017 (2017). DOI 10.1103/PhysRevD.96.084017
34. A. Abdujabbarov, B. Juraev, B. Ahmedov, Z. Stuchlík, *Astrophys Space Sci* **361**, 226 (2016). DOI 10.1007/s10509-016-2818-9
35. A. Abdujabbarov, M. Amir, B. Ahmedov, S.G. Ghosh, *Phys. Rev. D* **93**(10), 104004 (2016). DOI 10.1103/PhysRevD.93.104004
36. A.A. Abdujabbarov, L. Rezzolla, B.J. Ahmedov, *Mon. Not. R. Astron. Soc.* **454**, 2423 (2015). DOI 10.1093/mnras/stv2079
37. A. Abdujabbarov, B. Toshmatov, Z. Stuchlík, B. Ahmedov, *International Journal of Modern Physics D* **26**, 1750051-239 (2017). DOI 10.1142/S0218271817500511
38. F. Atamurotov, B. Ahmedov, A. Abdujabbarov, *Phys. Rev. D* **92**, 084005 (2015)
39. L. Amarilla, E.F. Eiroa, *Phys. Rev. D* **85**(6), 064019 (2012). DOI 10.1103/PhysRevD.85.064019
40. C. Bambi, K. Freese, *Phys. Rev. D* **79**(4), 043002 (2009). DOI 10.1103/PhysRevD.79.043002
41. C. Bambi, F. Caravelli, L. Modesto, *Physics Letters B* **711**, 10 (2012). DOI 10.1016/j.physletb.2012.03.068
42. C. Bambi, *Phys. Rev. D* **87**(10), 107501 (2013). DOI 10.1103/PhysRevD.87.107501
43. M. Ghasemi-Nodehi, Z. Li, C. Bambi, *European Physical Journal C* **75**, 315 (2015). DOI 10.1140/epjc/s10052-015-3539-x
44. P.V.P. Cunha, C.A.R. Herdeiro, E. Radu, H.F. Rúnarsson, *Physical Review Letters* **115**(21), 211102 (2015). DOI 10.1103/PhysRevLett.115.211102
45. S.W. Wei, Y.X. Liu, *Journal of Cosmology and Astroparticles* **11**, 063 (2013). DOI 10.1088/1475-7516/2013/11/063
46. R. Takahashi, *Publications of the Astronomical Society of Japan* **57**, 273 (2005). DOI 10.1093/pasj/57.2.273
47. T. Ohgami, N. Sakai, *Phys. Rev. D* **91**(12), 124020 (2015). DOI 10.1103/PhysRevD.91.124020
48. P.G. Nedkova, V.K. Tinchev, S.S. Yazadjiev, *Phys. Rev. D* **88**(12), 124019 (2013). DOI 10.1103/PhysRevD.88.124019
49. H. Falcke, F. Melia, E. Agol, *Astrophys. J. Lett.* **528**, L13 (2000). DOI 10.1086/312423
50. A. Grenzebach, V. Perlick, C. Lämmerzahl, *International Journal of Modern Physics D* **24**, 1542024 (2015). DOI 10.1142/S0218271815420249
51. R. Takahashi, *Astrophys. J.* **611**, 996 (2004). DOI 10.1086/422403
52. Z. Li, C. Bambi, *JCAP* **1**, 041 (2014). DOI 10.1088/1475-7516/2014/01/041
53. S.W. Wei, P. Cheng, Y. Zhong, X.N. Zhou, *JCAP* **8**, 004 (2015). DOI 10.1088/1475-7516/2015/08/004
54. U. Papnoi, F. Atamurotov, S.G. Ghosh, B. Ahmedov, *Phys. Rev. D* **90**(2), 024073 (2014). DOI 10.1103/PhysRevD.90.024073
55. C. Bambi, N. Yoshida, *Classical and Quantum Gravity* **27**(20), 205006 (2010). DOI 10.1088/0264-9381/27/20/205006
56. F. Atamurotov, A. Abdujabbarov, B. Ahmedov, *Phys. Rev. D* **88**(6), 064004 (2013). DOI 10.1103/PhysRevD.88.064004
57. F. Atamurotov, A. Abdujabbarov, B. Ahmedov, *Astrophys Space Sci* **348**, 179 (2013). DOI 10.1007/s10509-013-1548-5
58. N. Tsukamoto, Z. Li, C. Bambi, *Journal of Cosmology and Astroparticles* **6**, 043 (2014). DOI 10.1088/1475-7516/2014/06/043
59. A. Grenzebach, V. Perlick, C. Lämmerzahl, *Phys. Rev. D* **89**(12), 124004 (2014). DOI 10.1103/PhysRevD.89.124004
60. A. Abdujabbarov, F. Atamurotov, Y. Kucukakca, B. Ahmedov, U. Camci, *Astrophys. Space Sci.* **344**, 429 (2013). DOI 10.1007/s10509-012-1337-6
61. L. Amarilla, E.F. Eiroa, G. Giribet, *Phys. Rev. D* **81**(12), 124045 (2010). DOI 10.1103/PhysRevD.81.124045
62. L. Amarilla, E.F. Eiroa, *Phys. Rev. D* **87**(4), 044057 (2013). DOI 10.1103/PhysRevD.87.044057
63. K. Hioki, K.I. Maeda, *Phys. Rev. D* **80**(2), 024042 (2009). DOI 10.1103/PhysRevD.80.024042
64. Y. Mizuno, Z. Younsi, C.M. Fromm, O. Porth, M. De Laurentis, H. Olivares, H. Falcke, M. Kramer, L. Rezzolla, *Nature Astronomy* (2018). DOI 10.1038/s41550-018-0449-5
65. B. Paczynski, *Astrophys J.* **304**, 1 (1986). DOI 10.1086/164140
66. C. Alcock, C.W. Akerlof, R.A. Allsman, T.S. Axelrod, D.P. Bennett, S. Chan, K.H. Cook, K.C. Freeman, K. Griest, S.L. Marshall, H.S. Park, S. Perlmutter, B.A. Peterson, M.R. Pratt, P.J. Quinn, A.W. Rodgers, C.W. Stubbs, W. Sutherland, *Nature* **365**, 621 (1993). DOI 10.1038/365621a0
67. E. Aubourg, P. Bareyre, S. Bréhin, M. Gros, M. Lachièze-Rey, B. Laurent, E. Lesquoy, C. Magneville, A. Milsztajn, L. Moscoso, F. Queinnec, J. Rich, M. Spiro, L. Vigroux, S. Zylberajch, R. Ansari, F. Cavalier, M. Moniez, J.P. Beaulieu, R. Ferlet, P. Grison, A. Vidal-Madjar, J. Guibert, O. Moreau, F. Tajahmady, E. Maurice, L. Prévôt, C. Gry, *Nature* **365**, 623 (1993). DOI 10.1038/365623a0
68. A. Udalski, M. Szymanski, J. Kaluzny, M. Kubiak, W. Krzeminski, M. Mateo, G.W. Preston, B. Paczynski, *Acta Astronomica* **43**, 289 (1993)
69. B. Paczynski, *Annual Review of Astronomy and Astrophysics* **34**, 419 (1996). DOI 10.1146/annurev.astro.34.1.419
70. O.Y. Tsupko, G.S. Bisnovatyi-Kogan, *Gravitation and Cosmology* **15**, 184 (2009). DOI 10.1134/S0202289309020182
71. V. Bozza, M. Sereno, *Phys. Rev. D* **73**(10), 103004 (2006). DOI 10.1103/PhysRevD.73.103004
72. L.D. Landau, E.M. Lifshitz, *The Classical Theory of Fields, Course of Theoretical Physics, Volume 2* (Elsevier Butterworth-Heinemann, Oxford, 2004)
73. M. Visser, ArXiv e-prints, gr-qc: 0706.0622 (2007)
74. J.B. Hartle, K.S. Thorne, *Astrophys. J.* **153**, 807 (1968). DOI 10.1086/149707

- 75. V.L. Ginzburg, *The propagation of electromagnetic waves in plasmas. International Series of Monographs in Electromagnetic Waves*, Oxford: Pergamon, 1970, 2nd rev. and enl. ed. (1970)
- 76. S. Chandrasekhar, *An introduction to the study of stellar structure* (Dover Publications, New Haven, USA, 1939). Revised edition 1958
- 77. J. Binney, S. Tremaine, *Galactic dynamics*. Princeton, NJ, Princeton University Press, 1987, 747 p. (1987)
- 78. I.S. Gradshteyn, I.M. Ryzhik, A. Jeffrey, D. Zwillinger, *Table of Integrals, Series, and Products. Seventh Edition by I. S. Gradshteyn, I. M. Ryzhik, Alan Jeffrey, and Daniel Zwillinger*. Elsevier Academic Press, 2007. ISBN 012-373637-4 (2007)
- 79. G. Hinshaw, L.M. Krauss, *Astrophys. J* **320**, 468 (1987). DOI 10.1086/165564
- 80. M. Abramowitz, I.A. Stegun, *Handbook of Mathematical Functions*. New York: Dover, 1972 (1972)
- 81. G.S. Bisnovatyi-Kogan, O.Y. Tsupko, *Mon. Not. R. Astron. Soc* **404**, 1790 (2010). DOI 10.1111/j.1365-2966.2010.16290.x
- 82. T. Levi-Civita, E. Persico, M. Long, *The absolute differential calculus (calculus of tensors)* (Blackie, 1961). URL <https://books.google.com/books?id=CWQnAQAAIAAJ>
- 83. D. Lovelock, H. Rund, *Tensors, Differential Forms, and Variational Principles*. Dover Books on Mathematics (Dover Publications, 2012). URL <https://books.google.com/books?id=uUi8AQAAQBAJ>